

Combinatorial Design of Multimeric Chelating Peptoids for Selective Metal Coordination

Abel Ricano,^{†,‡} Ilya Captain,^{†,‡} Korey P. Carter,[†] Bryan P. Nell,[†] Gauthier J.-P. Deblonde,[†] and Rebecca J. Abergel^{†,§,*}

[†]Chemical Sciences Division, Lawrence Berkeley National Laboratory, Berkeley, CA 94720

[§]Department of Nuclear Engineering, University of California, Berkeley, CA 94720

E-mail: abergel@berkeley.edu

Supporting Information

I. Synthetic Procedures	4
II. LC and MS Spectra of Peptoids and Ln(III)-Peptoid Complexes	9
III. NMR Data	21
IV. UV-Vis Data	23
V. Luminescence Data	26
VI. Solution Thermodynamics	38
VII. References	41

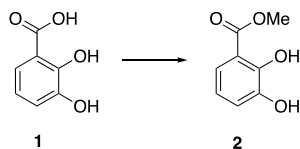
LIST OF FIGURES

Figure S1. Representative reversed-phase preparative HPLC trace of CCHC (13) peptoid.	9
Figure S2. LC-MS analysis of HHHC (1) peptoid.	10
Figure S3. LC-MS analysis of CHHH (2) peptoid.	10
Figure S4. LC-MS analysis of HCHH (3) peptoid.	11
Figure S5. LC-MS analysis of HHCH (4) peptoid.	11
Figure S6. LC-MS analysis of CHHC (5) peptoid.	11
Figure S7. LC-MS analysis of HHCC (6) peptoid.	12
Figure S8. LC-MS analysis of CCHH (7) peptoid.	12
Figure S9. LC-MS analysis of HCHC (8) peptoid.	12
Figure S10. LC-MS analysis of HCCH (9) peptoid.	13
Figure S11. LC-MS analysis of CHCH (10) peptoid.	13
Figure S12. LC-MS analysis of HCCC (11) peptoid.	13
Figure S13. LC-MS analysis of CHCC (12) peptoid.	14
Figure S14. LC-MS analysis of CCHC (13) peptoid.	14
Figure S15. LC-MS analysis of CCCH (14) peptoid.	14
Figure S16. LC-MS analysis of CCCC (15) peptoid.	15
Figure S17. LC-MS analysis of HHHH (16) peptoid.	15
Figure S18. LC-MS analysis of Eu:CHHC (5) complex.	16
Figure S19. LC-MS analysis of Eu:CHHH (2) complex.	16
Figure S20. HRMS data for peptoids (1)-(6).	17
Figure S21. HRMS data for peptoids (7)-(12).	18
Figure S22. HRMS data for peptoids (13)-(16).	19
Figure S23. TOF MS-MS analysis of peptoids (8), (9), and (15).	20
Figure S24. UV-Vis spectra for all ligands and respective Eu(III) and Tb(III) complexes.	25
Figure S25. Eu(III) emission spectra for peptoids (1)-(4)	29
Figure S26. Eu(III) emission spectra for peptoids (5)-(10)	29
Figure S27. Eu(III) emission spectra for peptoids (11)-(14)	30
Figure S28. Eu(III) emission spectra for peptoid (16) and 3,4,3-LI-(1,2-HOPO).	30
Figure S29. Eu(III) emission spectra for 3,4,3-LI(CAM) ₂ (1,2-HOPO) ₂ and 3,4,3-LI(1,2-HOPO) ₂ (CAM) ₂	31
Figure S30. High-resolution Eu(III) emission spectra for ⁵ D ₀ → ⁷ F ₂ hypersensitive transition.	32
Figure S31. Representative dilution curves used to determine quantum yield values.	35
Figure S32. Representative luminescence data for competition batch titrations.	38
Figure S33. Eu ³⁺ binding competition between (15) CCCC and 3,4,3-LI(CAM).	40
Figure S34. Eu ³⁺ binding and speciation with (15) CCCC (left) and (7) CCHH (right).	40

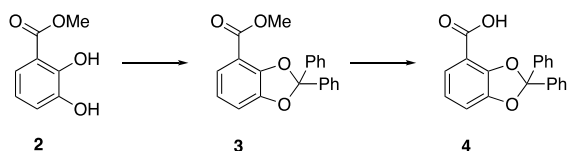
LIST OF TABLES

Table S1. Estimated quantum yield values	36
Table S2. Luminescence lifetimes for Eu(III) and Tb(III)-peptoid and 3,4,3-LI complexes	37
Table S3. Protonation and stability constants for selected ligands and complexes.....	39

I. Synthetic Procedures

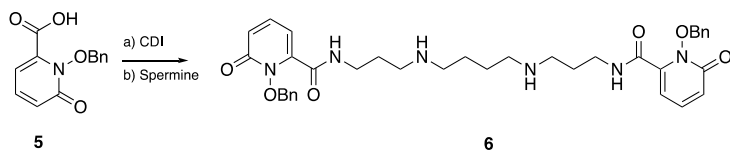


Methyl 2,3-dihydroxybenzoate, 2. A stirred suspension of **1** (8.06 g, 52.3 mmol) in 100 ml of methanol was treated with 2.00 ml of concentrated sulfuric acid. The suspension warmed and clarified 2 minutes after the addition. The reaction was equipped with a reflux condenser and was heated to 65°C overnight. The next morning the conversion was verified by LC-MS and the volatiles were removed under reduced pressure. The crude was partitioned between water (100 ml) and ethyl acetate (100 ml) and the aqueous layer was extracted with ethyl acetate (3x50 ml). The organic extracts were combined, dried over MgSO₄, and concentrated under reduced pressure. The crude was passed through a plug of silica using 10% ethyl acetate in hexanes as eluent. The eluent was concentrated under reduced pressure and dried under high vacuum for two hours to yield **2** (7.66 g, 45.6 mmol, 88%) as a white solid, the spectral properties of which matched previous reports.¹

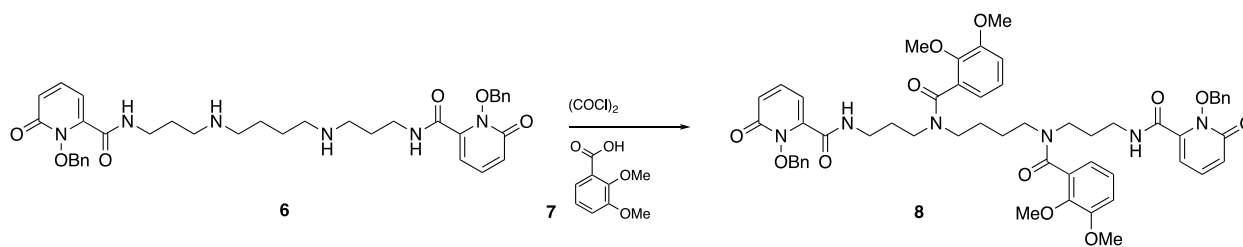


Methyl 2,2-diphenylbenzo[d][1,3]dioxole-4-carboxylate, 3. **2** (5.00 g, 29.7 mmol) was mixed with dichlorodiphenylmethane (8.56 ml, 44.6 mol) under an argon atmosphere, the resulting suspension was stirred and heated to 160°C for one hour. The mixture was allowed to cool to room temperature and was diluted with 100 ml of ethyl acetate. The solution was washed with sat. NaHCO₃ (30 ml) then brine (30 ml), dried over MgSO₄, then concentrated under reduced pressure. The ensuing greyish oil was dissolved in 30 ml of hot methanol (65°C) and was slowly cooled to 5°C, which resulted in the formation of white crystals. The crystals were a mixture of **3** and benzophenone dimethyl acetal that could not be easily separated; product was used as is for the subsequent step.

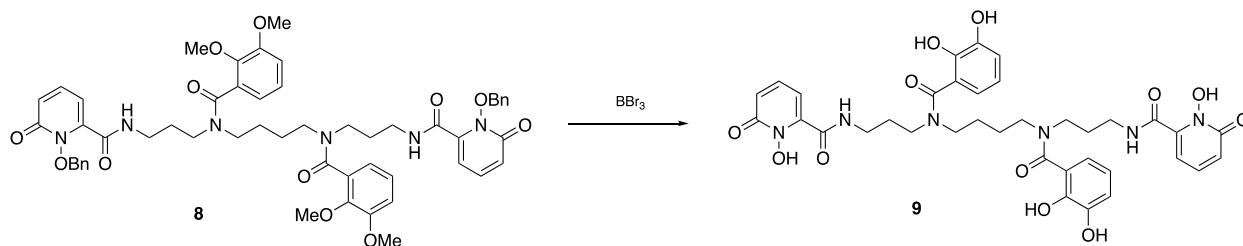
2,2-diphenylbenzo[d][1,3]dioxole-4-carboxylic acid, 4. The mixture from the previous step was dissolved in 100 ml of THF and was treated with 100 ml of 0.9 M LiOH. The emulsion was rapidly stirred and heated to reflux for five hours. Conversion was verified by LC-MS and the reaction was cooled to room temperature. The solution was neutralized with 10 % v/v aqueous acetic acid and was extracted with ethyl acetate (3x50 ml). The organic extracts were combined, dried over MgSO₄, and concentrated under reduced pressure. The crude was chromatographed using 25% ethyl acetate in hexanes as eluent. Volatiles were then removed under reduced pressure followed by high vacuum to yield **4** (7.6 g, 24.06 mmol, 81% over two steps) as a white solid, the spectral properties of which matched previous reports.¹



N,N'-((butane-1,4-diylbis(azanediyl))bis(propane-3,1-diyl))bis(1-(benzyloxy)-6-oxo-1,6-dihydropyridine-2-carboxamide), 6. **5** (350 mg, 1.43 mmol) was dissolved in 5 mL of N,N-dimethylformamide and the solution was treated with carbonyldiimidazole (231 mg, 1.43 mmol). The reaction was stirred at room temperature for 1 hour and treated with a solution of spermine (145 mg, 0.715 mmol in 3 mL of N,N-dimethylformamide); the resulting solution was stirred overnight at room temperature. The reaction was then diluted with 50 mL of 0.2 M aq. HCl and washed with ethyl acetate (15 mL x3). The aqueous solution was then made basic with brined 1.0 M KOH and extracted with dichloromethane (20 mL x 3). The dichloromethane washes were combined, dried over MgSO₄ and concentrated to yield the pure product as a clear yellow oil. (292 mg, 0.615 mmol, 86 % yield). ¹H NMR (300 MHz, CDCl₃) δ 7.52 (4H, m), 7.38 (6H, m), 7.27 (overlap with solvent residual peak, 2H expected), 6.66 (2H, dd, *J* = 9.3, 1.7 Hz), 6.39 (2H, dd, *J* = 6.8 Hz, 1.7 Hz), 5.29 (4H, s), 3.47 (4H, t, *J* = 6.0 Hz), 2.60 (4H, t, *J* = 6.0 Hz), 2.32 (4H, t, *J* = 6.0 Hz), 1.64 (8H, p, *J* = 6.0 Hz), 1.20 (4H, br s). MS-ESI (*m/z*) [*M* – *H*] Calcd. For C₃₆H₄₃N₆O₆, 655.3; found 655.0. MS-ESI (*m/z*) [*M* + *H*] Calcd. For C₃₆H₄₅N₆O₆, 657.3; found 657.0.

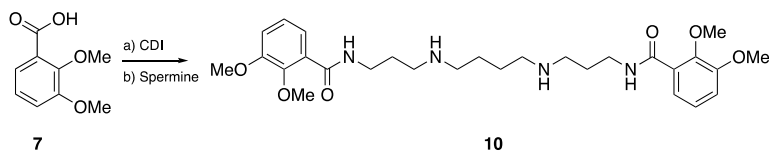


N,N'-((butane-1,4-diylbis((2,3-dimethoxybenzoyl)azanediyl))bis(propane-3,1-diyl))bis(1-(benzyloxy)-6-oxo-1,6-dihydropyridine-2-carboxamide), 8. Under an argon atmosphere, 2,3-dimethoxybenzoic acid (**7**, 550 mg, 3.02 mmol) was dissolved in toluene (5 mL), treated with (COCl)₂ (272 μL, 3.17 mmol) and cat. N,N-dimethylformamide, and stirred at 40°C for 1 hour. The volatiles were then removed on the manifold vacuum and the resulting brown oil was treated with **6** (900 mg, 1.37 mmol) as a solution in 10 mL dry tetrahydrofuran and triethylamine (440 μL, 3.17 mmol). The resulting mixture was stirred at 50°C for 3 hours. Upon cooling to room temperature the solids were filtered off and volatiles were removed under reduced pressure to yield a crude orange oil. The crude product was chromatographed on silica using 5% methanol in dichloromethane as eluent (*R*_f = 0.35). The desired fractions were concentrated on a rotary evaporator and stripped of volatiles on the manifold vacuum to yield **8** as a solid white foam (841 mg, 0.854 mmol, 62 % yield). ¹H NMR (300 MHz, CDCl₃) δ 7.89 (1H, m), 7.73 (1H, t, *J* = 3.7 Hz), 7.58 (2H, br s), 7.29-7.50 (8H, m), 7.24 (1H, br s), 6.99-7.12 (2H, m), 6.84-6.96 (2H, m), 6.72-6.76 (2H, m), 6.53-6.69 (2H, m), 6.33 (1H, ddd, *J* = 11.1, 4.0, 1.0 Hz), 6.24 (1H, m), 5.22-5.49 (4H, br s), 3.72-3.91 (12H, br s), 3.56 (2H, br s), 2.66-3.43 (10H, br s), 0.96-1.91 (8H, br s).



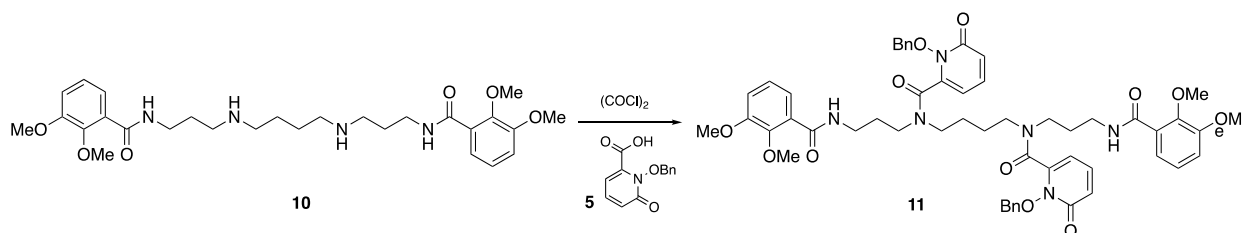
[3,4,3-LI(1,2-HOPO)₂(CAM)₂] [also abbreviated 3,4,3-LI(HCCH)]

N,N'-((butane-1,4-diylbis((2,3-dihydroxybenzoyl)azanediyl))bis(propane-3,1-diyl))bis(1-hydroxy-6-oxo-1,6-dihydropyridine-2-carboxamide), 9. **8** (530 mg, 0.538 mmol) was dissolved in 10 mL of dichloromethane and was treated with boron tribromide (510 μ L, 5.38 mmol). The reaction was capped and stirred overnight at 50°C. The excess reagent was then quenched by slow addition of 10 mL of methanol. The solvent was then removed on a rotary evaporator and the residue dissolved in 21 mL of water with a minimal amount of acetonitrile to obtain a clear solution. The product containing solution was then purified on preparative HPLC using a gradient of 10 \rightarrow 30 % acetonitrile in water + 0.1 % trifluoroacetic acid in 3 portions. The fractions containing the product were combined and stripped of trifluoroacetic acid on a GeneVac evaporator. The water was removed by lyophilization yielding **9** as a fluffy white solid (128 mg, 0.171 mmol, 32 % yield). ¹H NMR (500 MHz, (CD₃)₂SO) δ 9.58 (2H, br s), 8.79 (1H, t, J = 5.5 Hz), 8.63 (1H, br s), 7.38 (2H, br s), 6.78 (2H, d, J = 7.4 Hz), 6.65 (2H, br s), 6.57 (2H, m), 6.44 (1H, br s), 6.33 (1H, m), 6.04 (1H, br s), 4.88 (4H, br s), 2.88-3.58 (10H, overlapping signals), 1.11-1.84 (8H, overlapping signals). HRMS-ESI (m/z) [$M - H$] Calcd. For C₃₆H₃₉N₆O₁₂, 747.2626; found 747.1935.

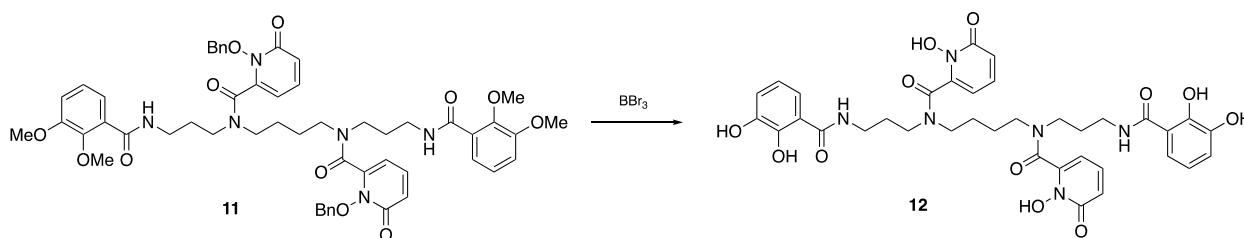


N,N'-((butane-1,4-diylbis(azanediyl))bis(propane-3,1-diyl))bis(2,3-dimethoxybenzamide),

10. 2,3-dimethoxybenzoic acid (**7**, 224 mg, 1.23 mmol) was dissolved in 4 mL of N,N-dimethylformamide and was treated with carbonyldiimidazole (199 mg, 1.23 mmol). The resulting mixture was stirred at room temperature for 1.5 hours and then treated with a solution of spermine (124 mg, 0.615 mmol in 3 mL of N,N-dimethylformamide); the resulting solution was stirred overnight at room temperature. The reaction was then diluted with 50 mL of 0.2 M aq. HCl and washed with ethyl acetate (15 mL x 3). The aqueous solution was made basic with brined 1.0 M KOH and extracted with dichloromethane (3x20 mL). The dichloromethane washes were combined, dried over MgSO₄ and concentrated to yield a clear yellow oil, which was used without further purification (284 mg). MS-ESI (m/z) [$M - H$] Calcd. For C₂₈H₄₁N₄O₆, 529.3; found 529.0. MS-ESI (m/z) [$M + H$] Calcd. For C₂₈H₄₃N₄O₆, 531.3; found 531.0.



N,N'-(butane-1,4-diyl)bis(1-(benzyloxy)-N-(3-(2,3-dimethoxybenzamido)propyl)-6-oxo-1,6-dihydropyridine-2-carboxamide), 11. Under an argon atmosphere, Bn-1,2-HOPO, **5**, (916 mg, 3.74 mmol) was suspended in toluene (20 mL), treated with (COCl)₂ (350 μ L, 4.08 mmol) with cat. N,N-dimethylformamide, and was stirred at 40°C for 1 hour. Volatiles were then removed on the manifold vacuum and the resulting brown oil was dissolved in tetrahydrofuran (10 mL) and treated with **10** (901 mg, 1.70 mmol) in a solution of 10 mL dry tetrahydrofuran and triethylamine (566 μ L, 4.08 mmol). The resulting mixture was stirred at 50°C for 3 hours. The volatiles were then removed under reduced pressure and the residue was suspended in ethyl acetate. The suspension was transferred into a separatory funnel and was washed with 1.0 M aq. HCl (15 mL x 3) followed by 1.0 M aq. NaOH (3x15 mL). The organic phase was dried over MgSO₄ and concentrated on a rotary evaporator. The resulting crude was purified by column chromatography using 5% methanol in dichloromethane as eluent (R_f = 0.40). The desired fractions were combined, concentrated on a rotary evaporator, and dried under vacuum yielding **11** as a solid white foam (837 mg, 0.850 mmol, 50% yield). ¹H NMR (300 MHz, CDCl₃) δ 8.27 (1H, m), 7.92 (1H, m), 7.69 (1H, m), 7.42-7.62 (6H, m), 7.26-7.41 (8H, m), 7.08-7.19 (3H, m), 7.04 (2H, m), 6.68 (1H, m), 6.53 (1H, m), 5.88-6.05 (2H, m), 5.56-5.64 (2H, m), 5.02 (2H, m), 3.96 (3H, m), 3.89 (6H, m), 3.78 (3H, m), 2.90-3.60 (12H, m), 1.55-1.87 (8H, br s).



[3,4,3-LI(CAM)₂(1,2-HOPO)₂] [also abbreviated 3,4,3-LI(CHHC)]

N,N'-(butane-1,4-diyl)bis(N-(3-(2,3-dihydroxybenzamido)propyl)-1-hydroxy-6-oxo-1,6-dihydropyridine-2-carboxamide), 12. **11** (599 mg, 0.608 mmol) was dissolved in 10 mL of dichloromethane and treated with boron tribromide (577 μ L, 6.08 mmol). The reaction was capped and stirred overnight at 50°C. The next day the excess reagent was quenched by slowly adding 10 mL of methanol. The solvent was then removed on a rotary evaporator and the residue was dissolved in 21 mL of water with a minimal amount of acetonitrile to obtain a clear solution. The product containing solution was then purified on preparative HPLC using a gradient of 10 \rightarrow 30 % acetonitrile in water + 0.1 % trifluoroacetic acid in 3 portions. The fractions containing the product were combined and stripped of trifluoroacetic acid on a GeneVac evaporator. The water was removed by lyophilization yielding **12** as a fluffy white solid (142 mg, 0.190 mmol,

31% yield). ^1H NMR (500 MHz, $(\text{CD}_3)_2\text{SO}$) δ 12.71 (2H, br s), 9.14 (2H, br s), 8.79 (1H, q, $J = 6.7$ Hz), 8.66 (1H, dt, $J = 9.5, 5.5$ Hz), 7.37 (1H, ddd, $J = 19.3, 9.1, 6.9$ Hz), 7.27 (1H, dt, $J = 8.2, 1.5$ Hz), 7.18 (1H, ddd, $J = 13.7, 6.9, 4.6$ Hz), 7.12 (1H, ddd, $J = 8.2, 4.6, 1.4$ Hz), 6.90 (2H, m), 6.68 (1H, td, $J = 8.0, 3.5$ Hz), 6.65 (1H, td, $J = 8.0, 3.5$ Hz), 6.52 (1H, dt, $J = 9.1, 1.7$ Hz), 6.35 (1H, ddd, $J = 9.1, 3.7, 1.6$ Hz), 6.18 (1H, ddd, $J = 29.4, 6.9, 1.7$ Hz), 6.12 (1H, ddd, $J = 6.6, 5.1, 1.6$ Hz), 3.41-3.65 (4H, br s), 2.97-3.24 (8H, br s), 1.36-1.88 (8H, br s). ^{13}C NMR (125 MHz, $(\text{CD}_3)_2\text{SO}$) δ 170.3, 170.2, 161.8, 161.6, 158.8, 158.5, 157.9, 157.7, 150.1, 150.1, 146.7, 146.6, 142.4, 142.3, 138.2, 137.8, 119.6, 119.3, 118.4, 118.3, 117.5, 117.5, 115.4, 115.3, 102.5, 102.2, 47.8, 47.7, 37.1, 37.0, 36.8, 36.8, 28.0, 27.2, 25.3, 24.2. HRMS-ESI (m/z) $[\text{M} - \text{H}]$ Calcd. For $\text{C}_{36}\text{H}_{39}\text{N}_6\text{O}_{12}$, 747.2626; found 747.1909.

II. LC and MS Spectra of Peptoids and Ln(III)-Peptoid Complexes

Reversed-Phase Preparative HPLC Method

Time (min)	% Acetonitrile (with 0.1 % TFA)	% Water (with 0.1 % TFA)	Flow (ml/min)
0	5	95	10
5	5	95	10
25	20	80	15
70	40	20	15
75	90	10	15
80	5	95	15
85	5	95	15

Most peptoids had peak maxima between 20 and 40 minutes, methods were typically terminated once the target material was collected. The column was flushed with 50/50 solvent composition for 5 minutes and equilibrated to initial condition for at least 20 minutes before every injection; insufficient equilibration leads to low column loading and very low yields. Peptoids with higher CAM compositions tended to be less polar and thus came out later than HOPO-heavy analogs.

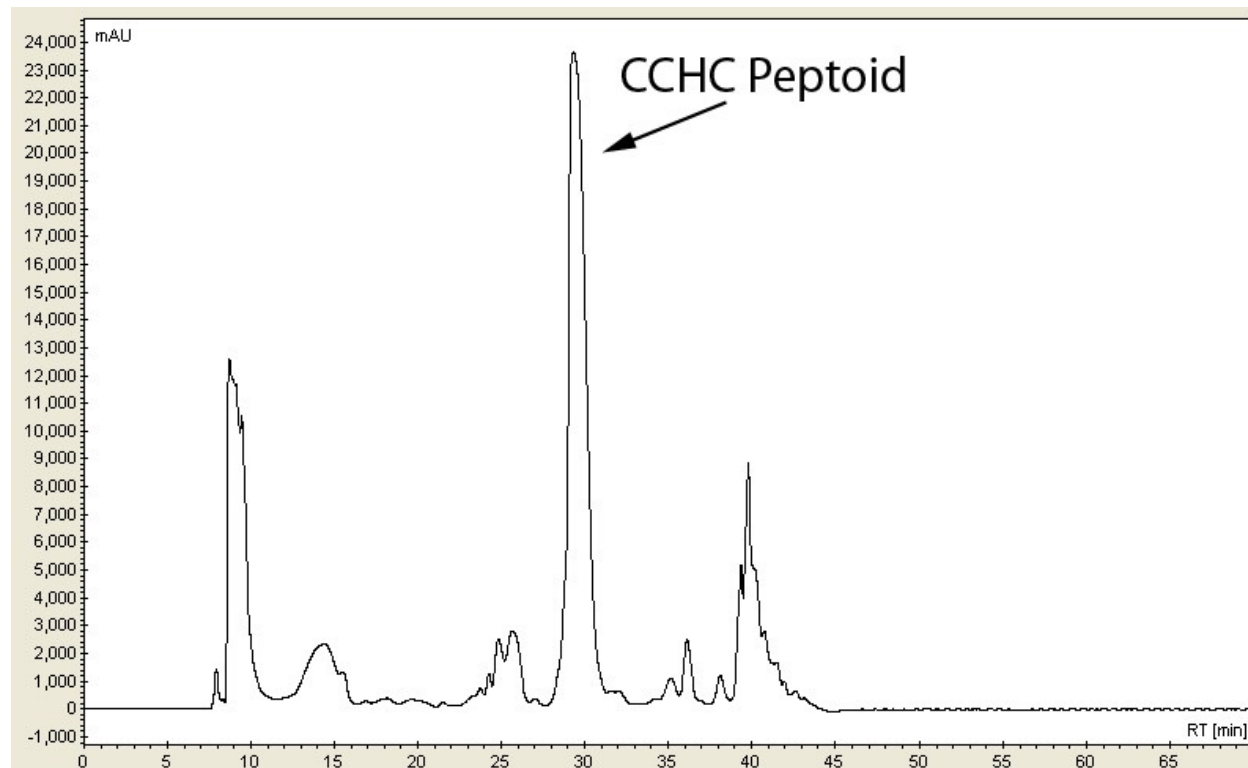


Figure S1. Representative reversed-phase preparative HPLC trace of CCHC (13) peptoid.

Peptoid LC-MS of purified peptoids:

LC traces of peptoids A@320. Ion counts along the entire peak including shoulders were used to generate mass spectra. Spectra were obtained in negative mode on an Agilent 6530 mass spectrometer. MS labels from left to right.

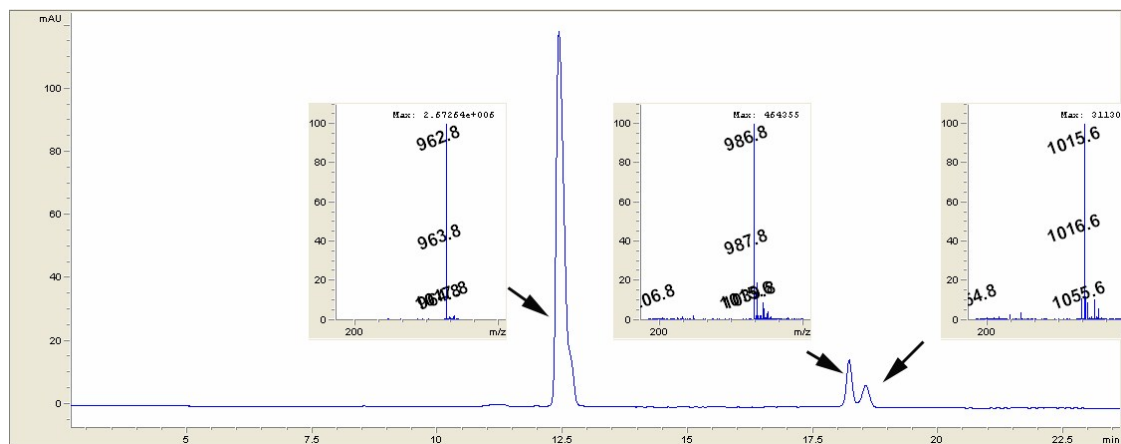


Figure S2. LC-MS analysis of **HHHC** (1) peptoid. MS1: free peptoid, MS2: peptoid-Na, MS3: peptoid-Fe and peptoid-Fe-K.

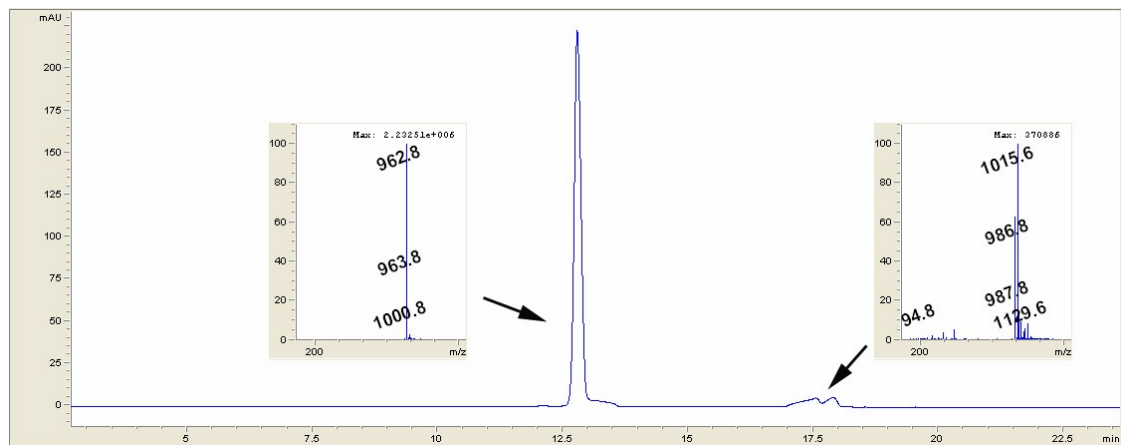


Figure S3. LC-MS analysis of **CHHH** (2) peptoid. MS1: free peptoid and peptoid-K, MS2: peptoid-Na, peptoid-Fe, and possible impurity.

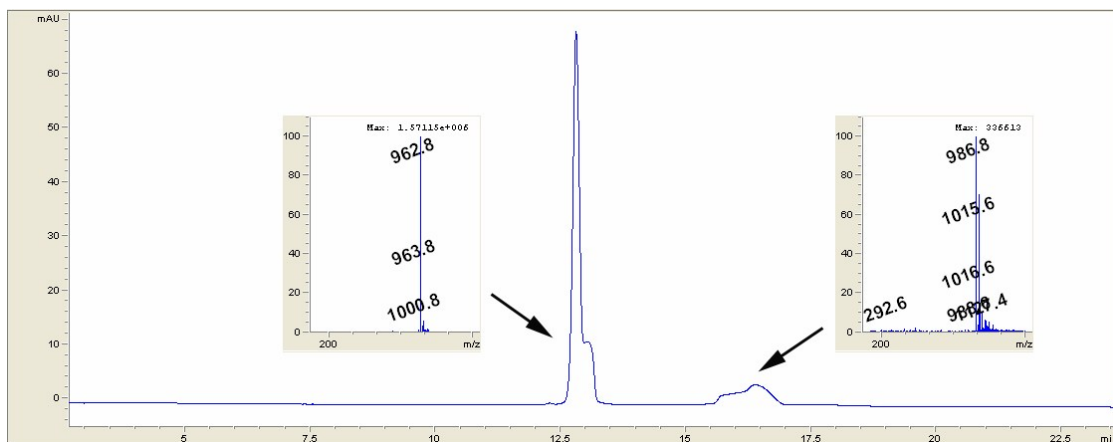


Figure S4. LC-MS analysis of **HCHH** (3) peptoid. MS1: free peptoid and peptoid-K, MS2: peptoid-Na, peptoid-Fe.

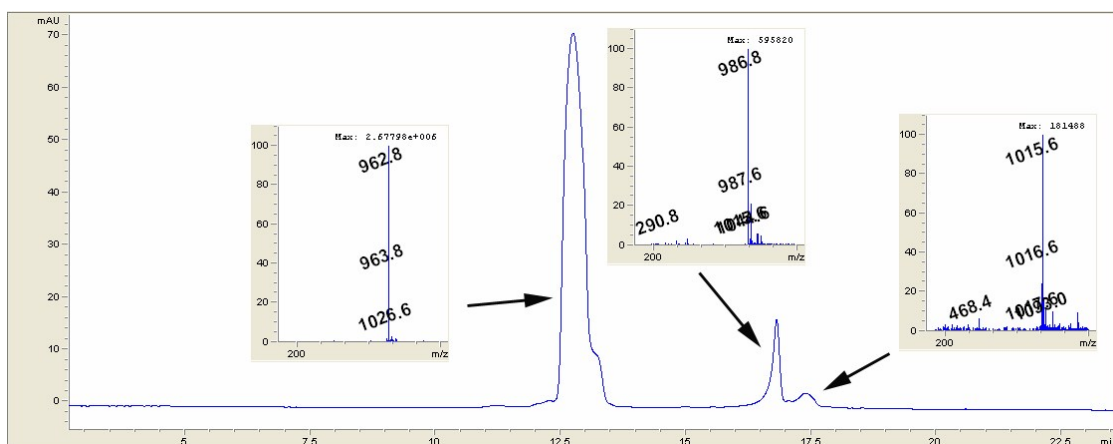


Figure S5. LC-MS analysis of **HHCH** (4) peptoid. MS1: free peptoid and possible impurity, MS2: peptoid-Na, MS3: Peptoid-Fe.

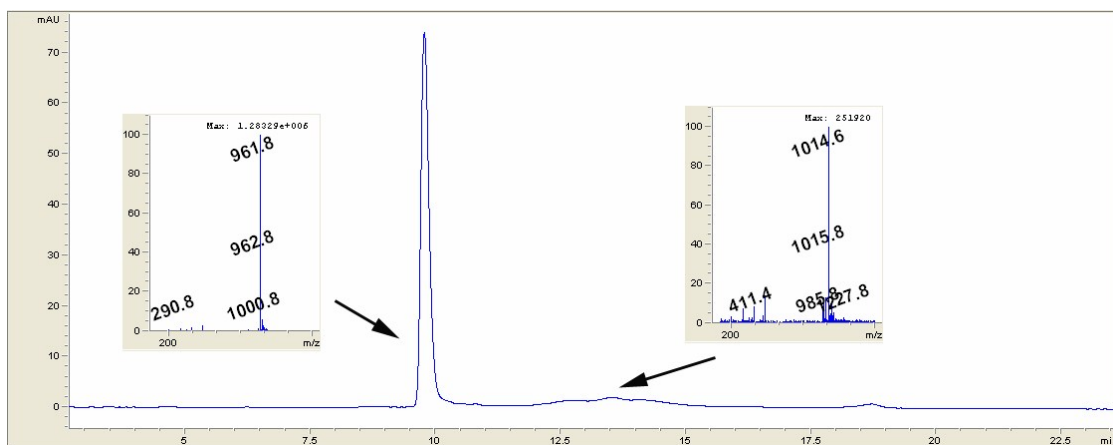


Figure S6. LC-MS analysis of **CHHC** (5) peptoid. MS1: free peptoid only and peptoid-K, MS2: peptoid-Na and peptoid-Fe.

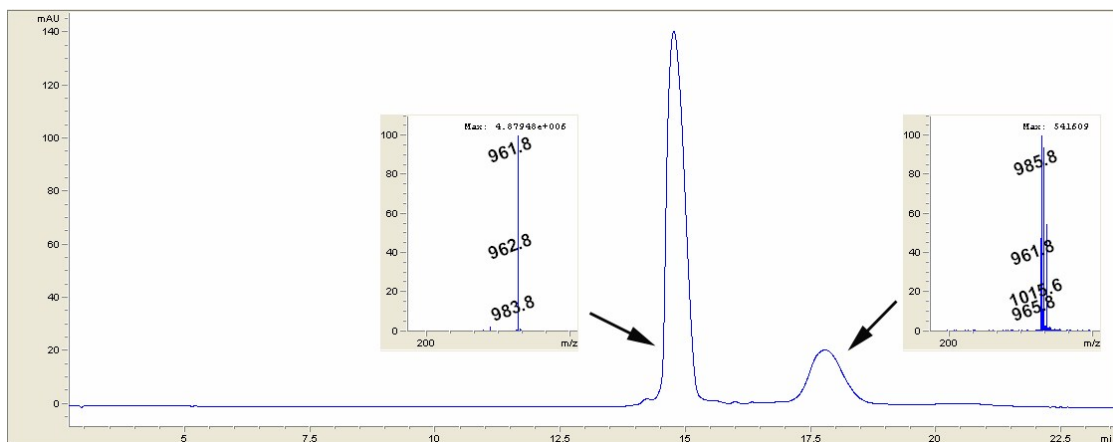


Figure S7. LC-MS analysis of **HHCC** (6) peptoid. MS1: free peptoid and peptoid-Na, MS2: peptoid-Na, free peptoid, and peptoid-Fe.

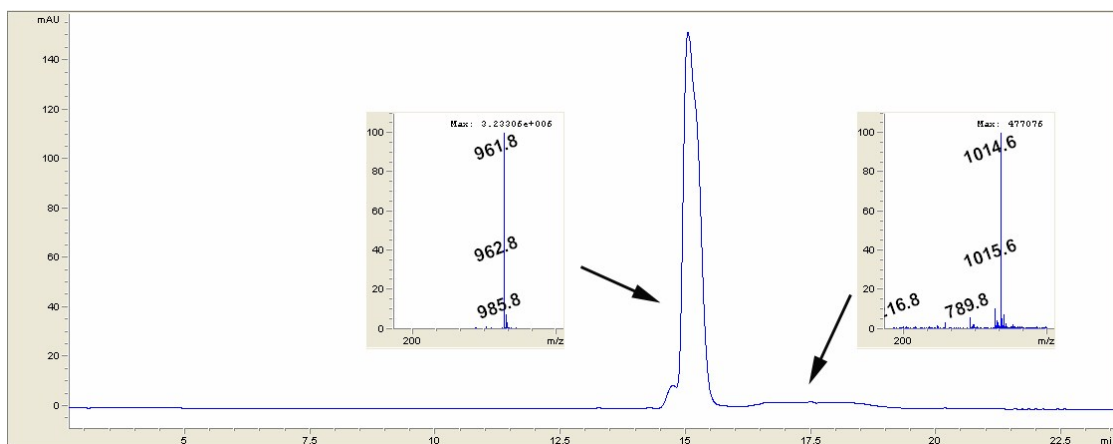


Figure S8. LC-MS analysis of **CCHH** (7) peptoid. MS1: free peptoid and peptoid-Na, MS2: Peptoid-Fe and possible trimer.

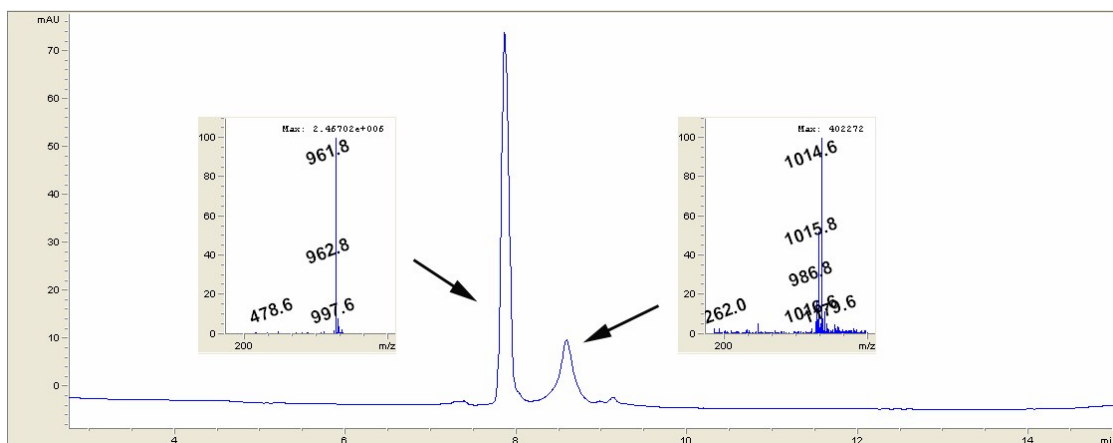


Figure S9. LC-MS analysis of **HCHC** (8) peptoid. MS1: free peptoid, MS2: peptoid-Fe and peptoid-Na.

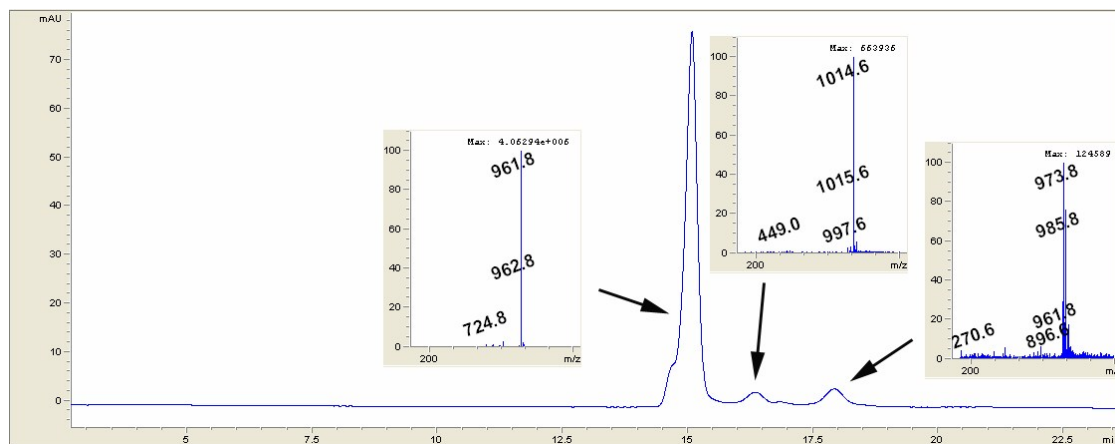


Figure S10. LC-MS analysis of **HCCH (9)** peptoid. MS1: free peptoid and small amount trimer, MS2: peptoid-Fe, MS3: peptoid-Na and possible fragments.

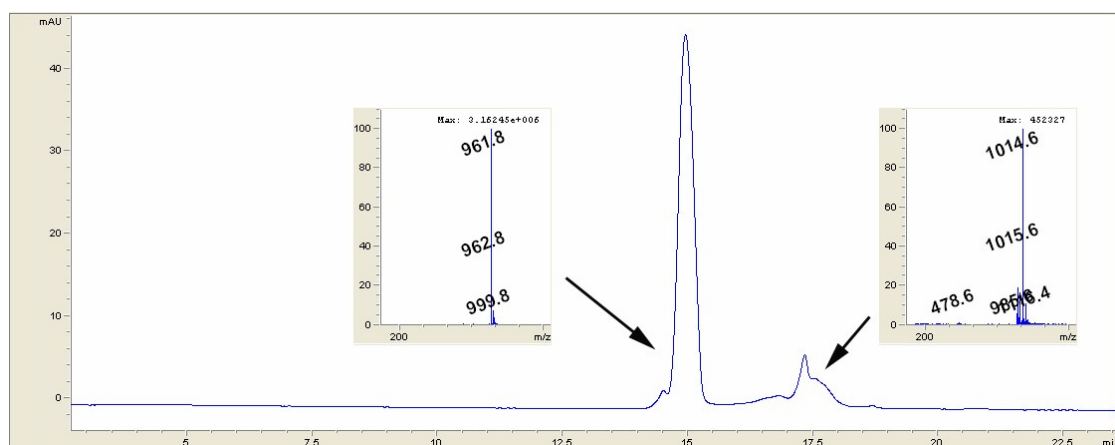


Figure S11. LC-MS analysis of **CHCH (10)** peptoid. MS1: free peptoid and peptoid-K, MS2: peptoid-Fe.

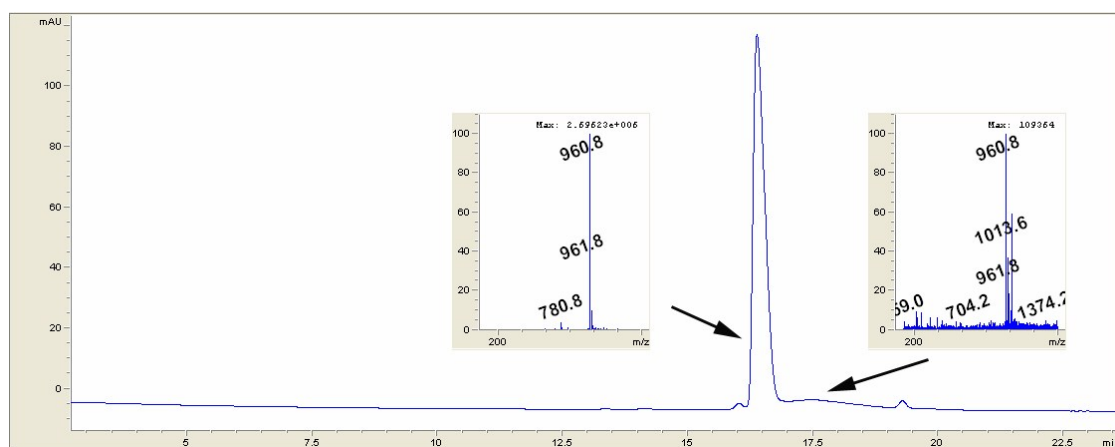


Figure S12. LC-MS analysis of **HCCC (11)** peptoid. MS1: free peptoid and trimer-Fe trace, MS2: free peptoid and peptoid-Fe

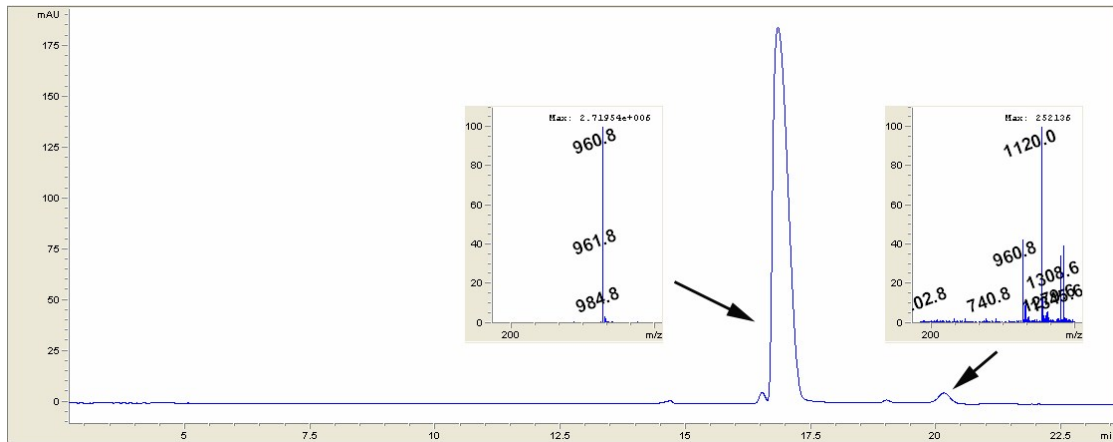


Figure S13. LC-MS analysis of CHCC (12) peptoid. MS1: free peptoid and peptoid-Na, MS2: free peptoid and unidentified masses.

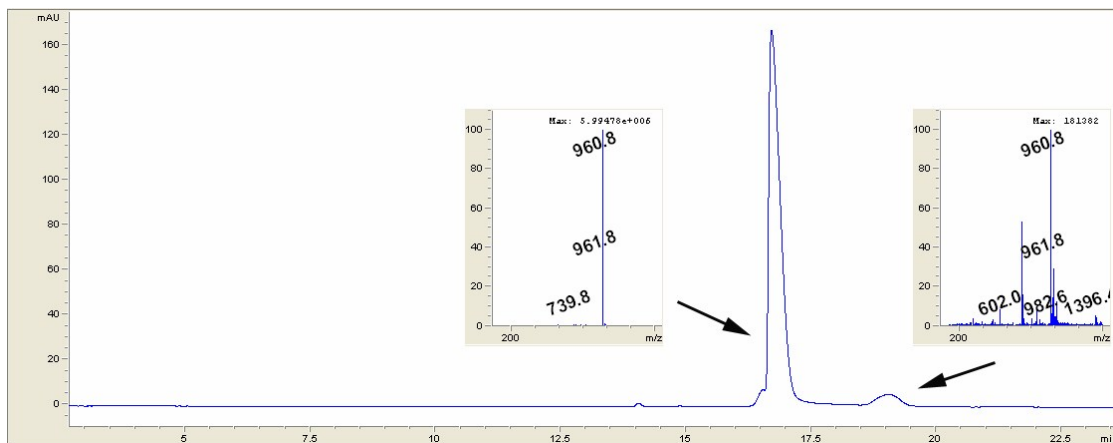


Figure S14. LC-MS analysis of CCHC (13) peptoid. MS1: free peptoid, MS2: free peptoid and peptoid-Na

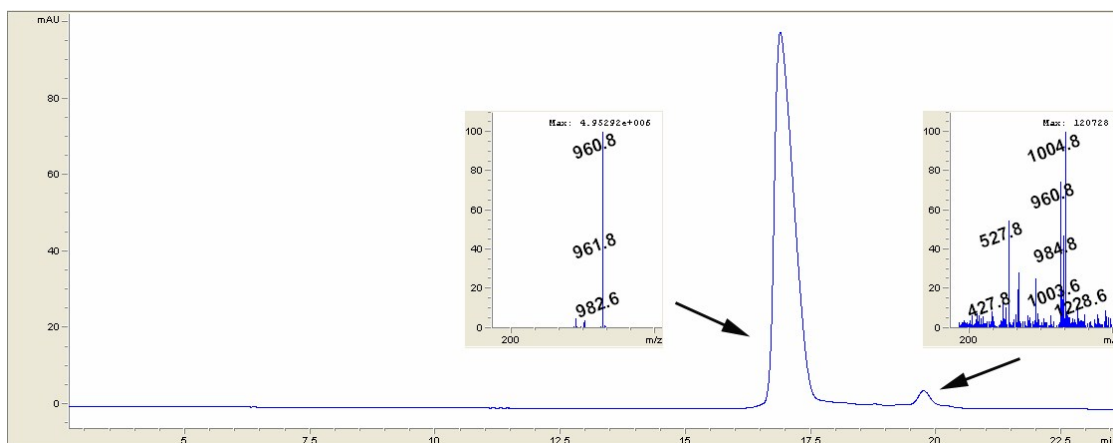


Figure S15. LC-MS analysis of CCCH (14) peptoid. MS1: free peptoid and peptoid-Na, MS2: free peptoid and peptoid-K/Na

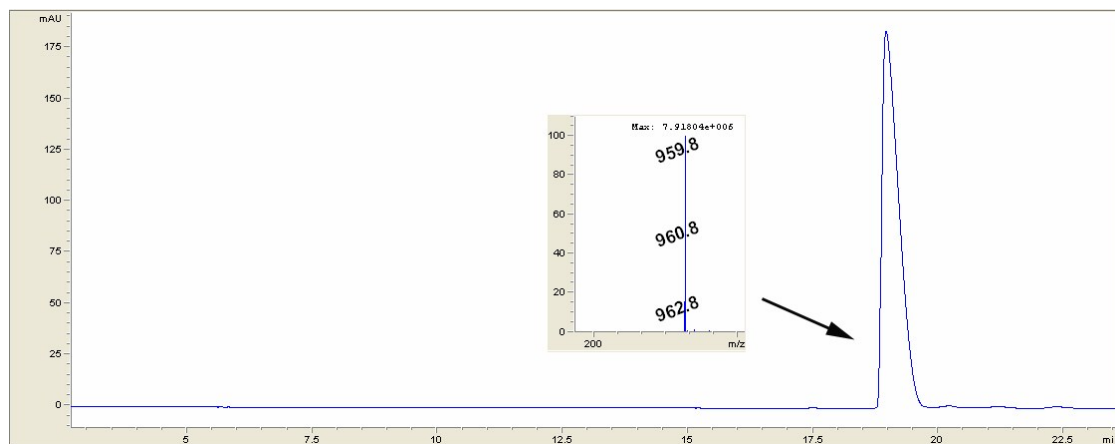


Figure S16. LC-MS analysis of CCCC (15) peptoid. Free peptoid only by MS.

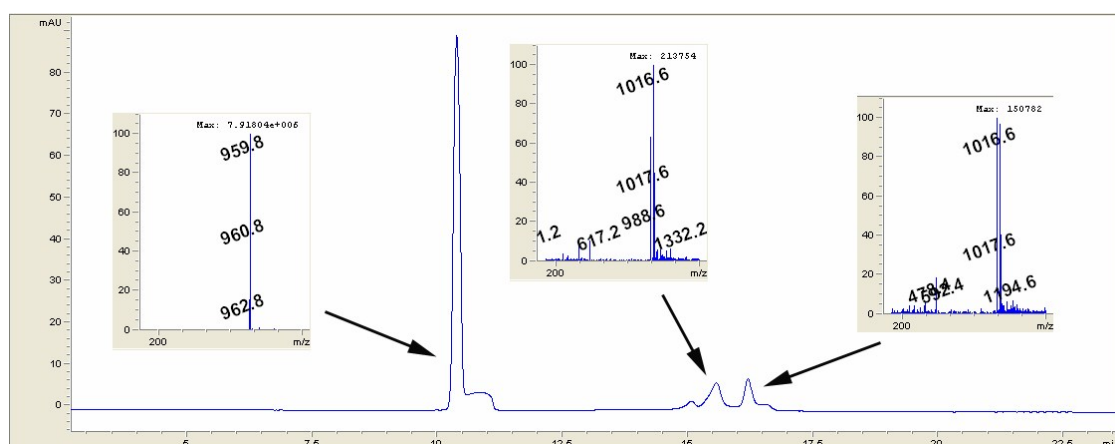


Figure S17. LC-MS analysis of HHHH (16) peptoid. MS1: free peptoid, MS2: peptoid-Fe/Na, MS3: Peptoid-Fe-Na

Mass Spectrometry for Eu-Peptoid Complex

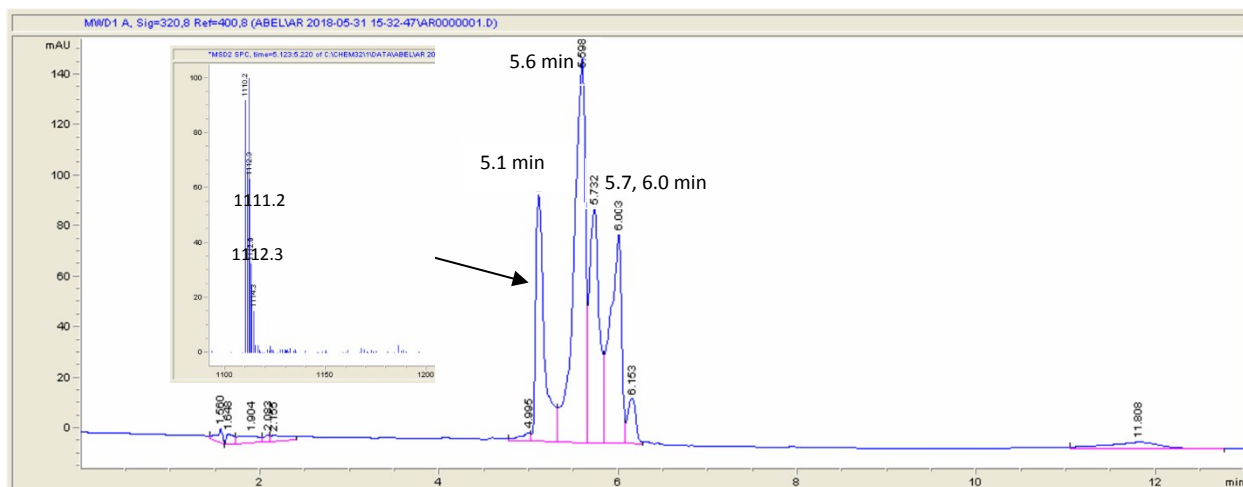


Figure S18. LC-MS analysis of Eu:CHHC (5) complex. Predicted mass of $M - H = 963$, $M + \text{Eu} - 4H = 1112$, $M + \text{Fe} - 4H = 1015$. Peaks at 5.1 min and 5.7 min correspond to europium complex and free ligand, respectively. LC trace monitored at 320 nm with mass spectra included as inset.

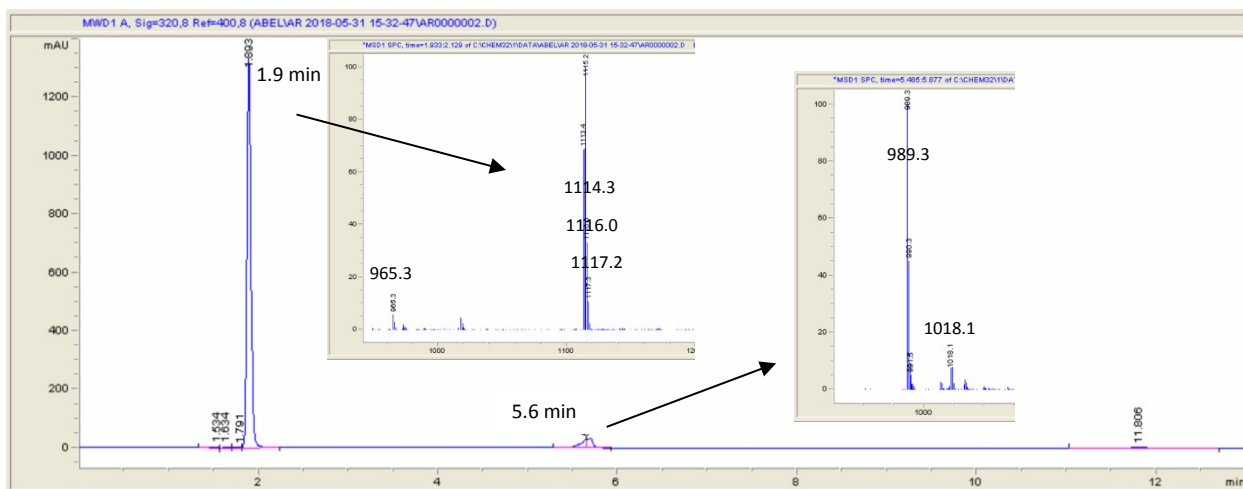


Figure S19. LC-MS analysis of Eu:CHHH (2) complex. Predicted mass of $M + H = 965$, $M + \text{Eu} - 2H = 1115$, $M + \text{Fe} - 2H = 1018$. Peak at a retention time of 1.9 min corresponds to the europium complex. LC trace monitored at 320 nm with mass spectra included as insets.

High Resolution Mass Spectrometry Data

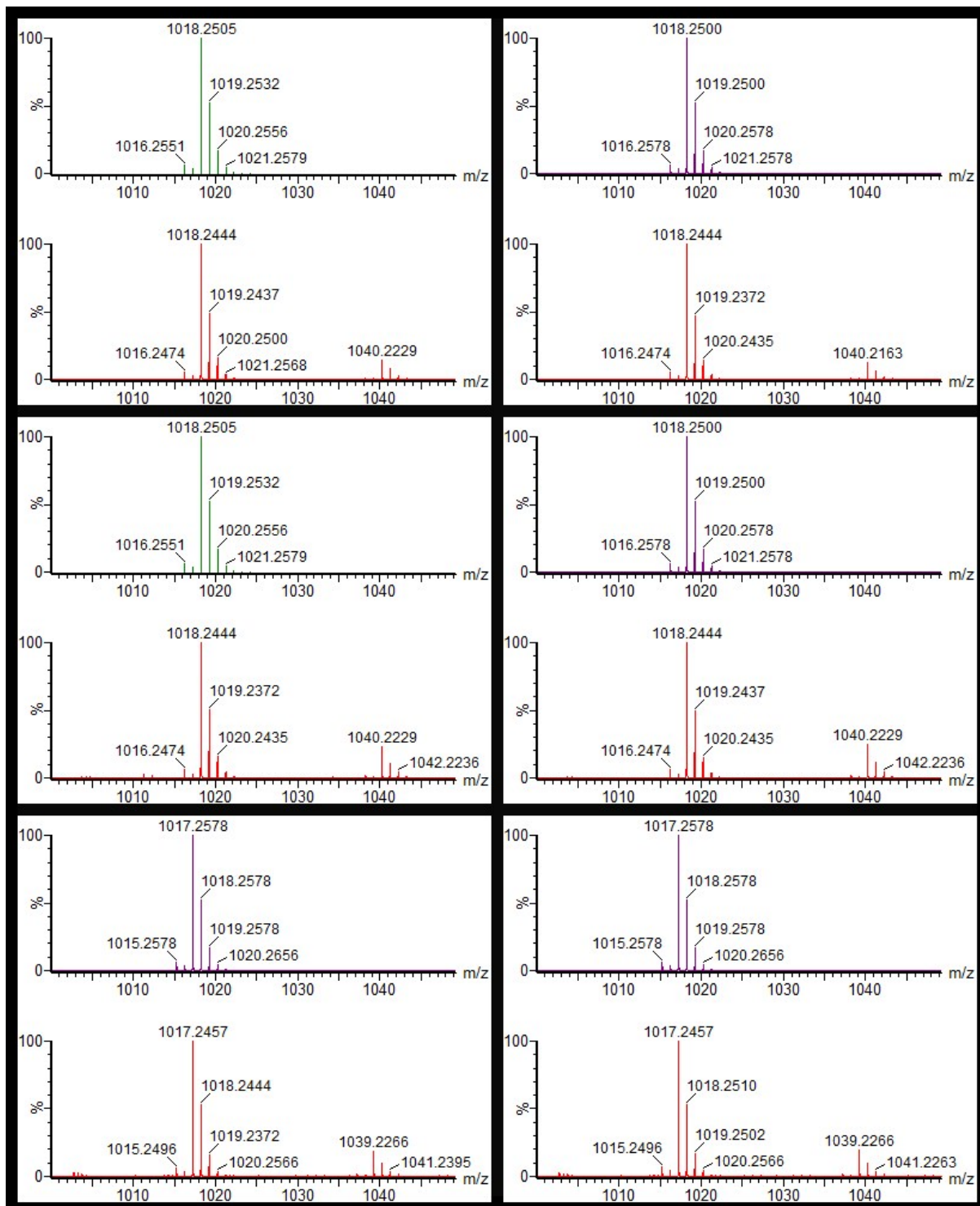


Figure S20. HRMS data for peptoids (1)-(6). Calculated (top) and observed (bottom) negative mode high resolution mass spectra of 1:1 Fe^{3+} -peptoid complexes where from left to right and top to bottom peptoids are HHC (1), CHH (2), HCH (3), HHCH (4), CHHC (5), and HHCC (6), respectively.

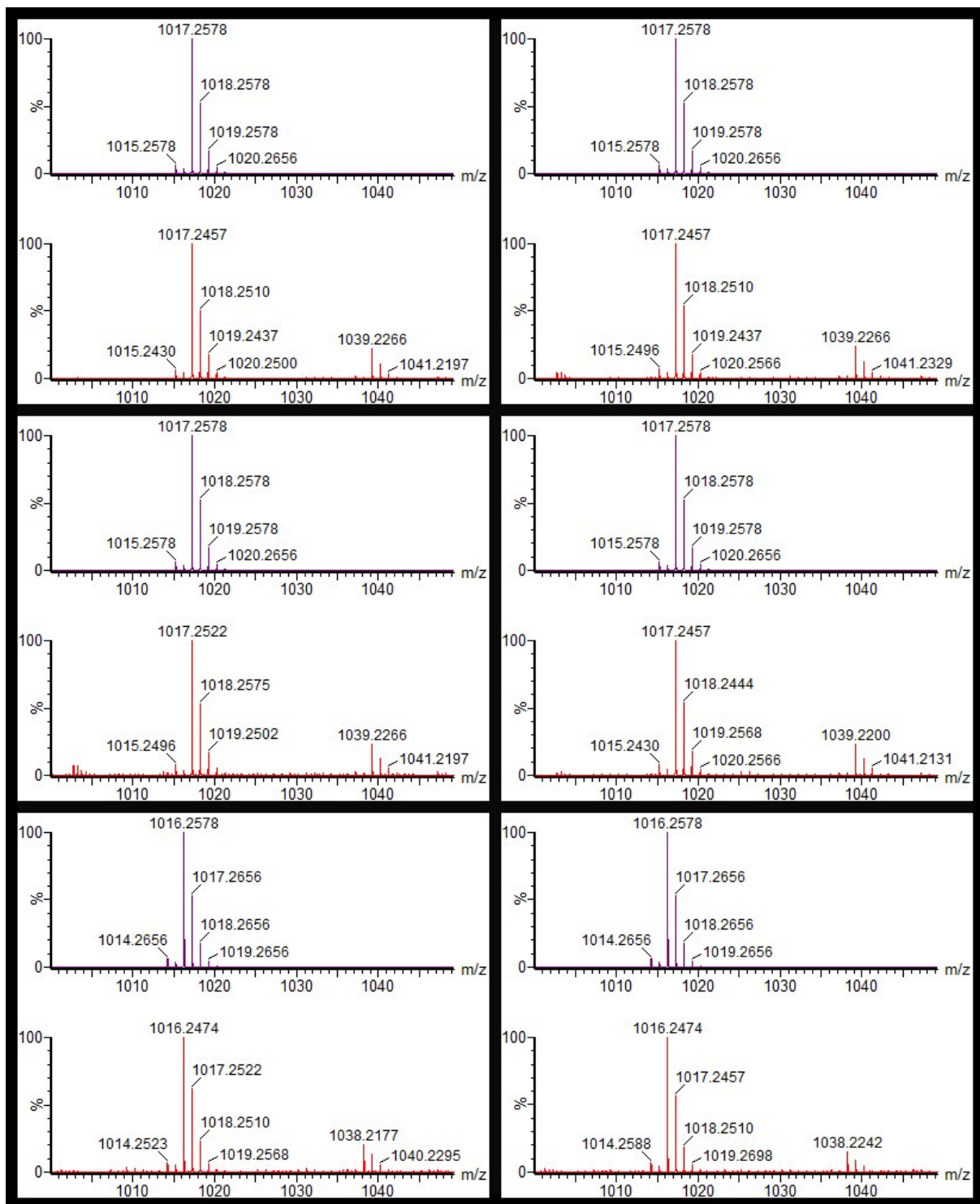


Figure S21. HRMS data for peptoids (7)-(12). Calculated (top) and observed (bottom) negative mode high resolution mass spectra of 1:1 Fe^{3+} -peptoid complexes where from left to right and top to bottom peptoids are CCHH (7), HCHC (8), HCCH (9), CHCH (10), HCCC (11), and CHCC (12), respectively.

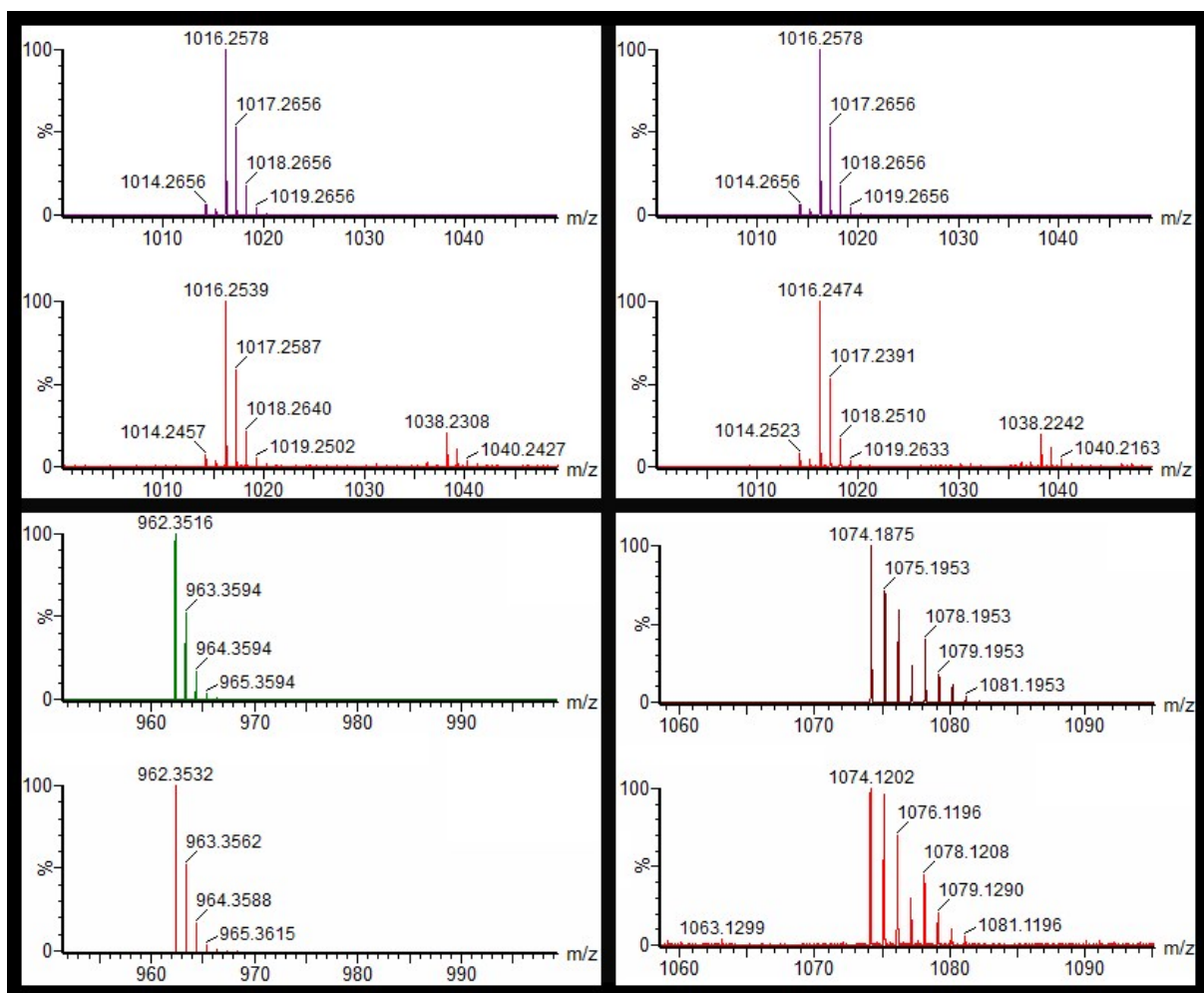


Figure S22. HRMS data for peptoids (13)-(16). Calculated (top) and observed (bottom) negative mode high resolution mass spectra of 1:1 Fe³⁺-peptoid complexes with CCHC (13) and CCCH (14) as well as calculated and observed spectra with CCCC (15) (uncomplexed) and HHHH (16):Zr:Na.

TOF MS-MS of Select Peptoids

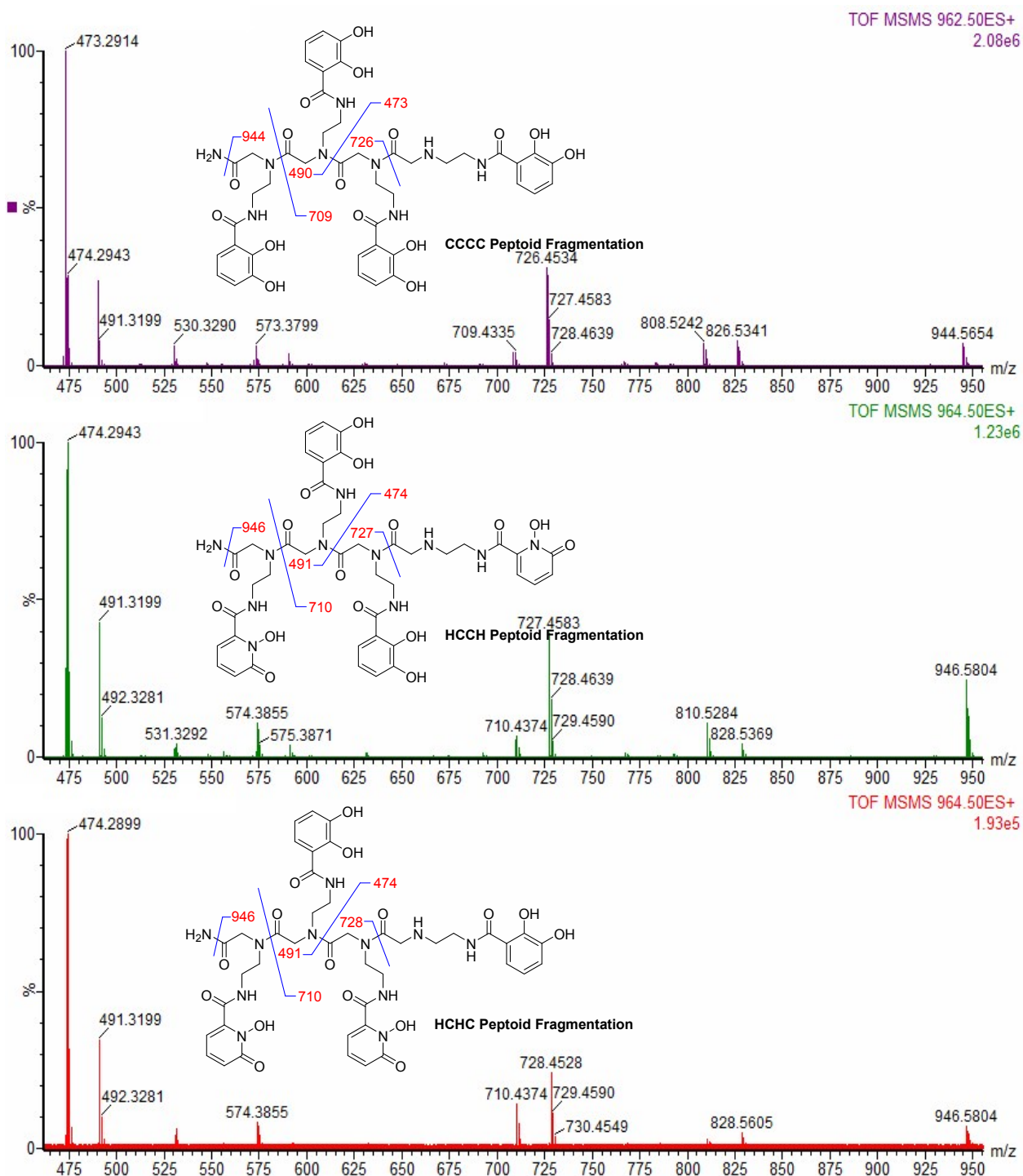
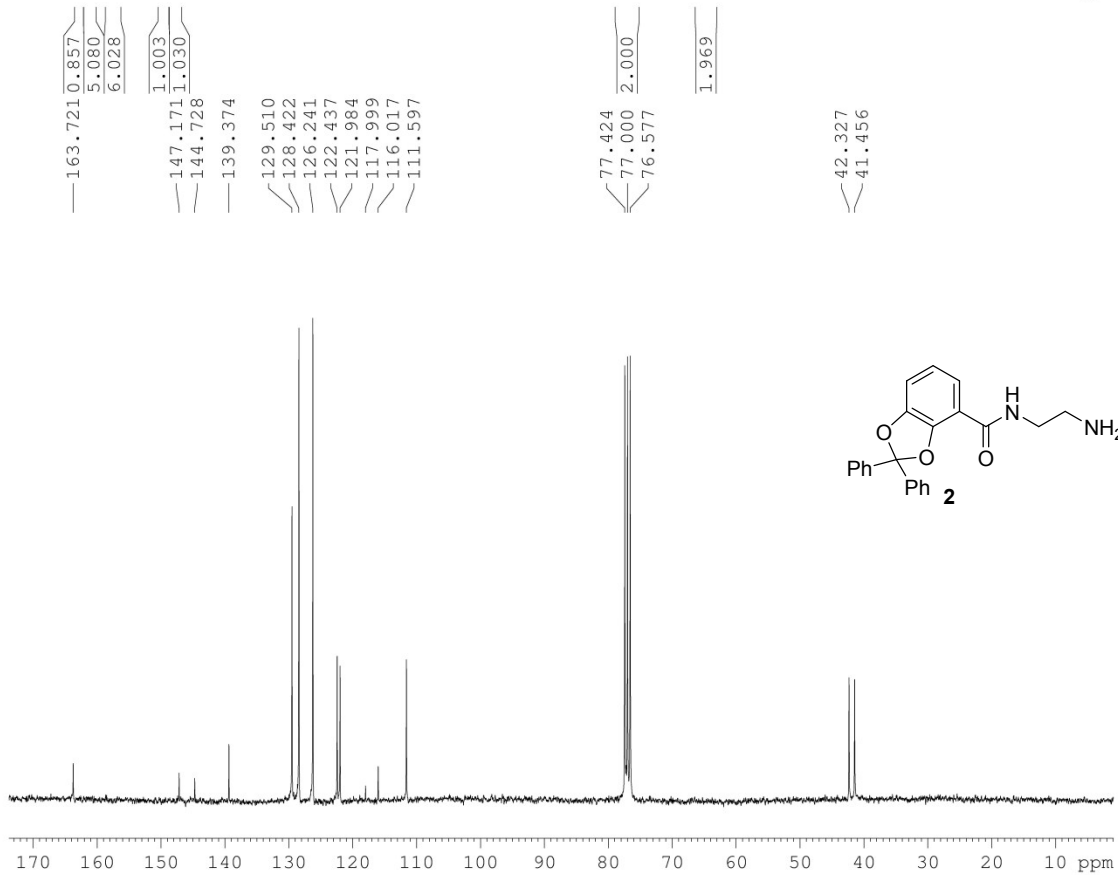
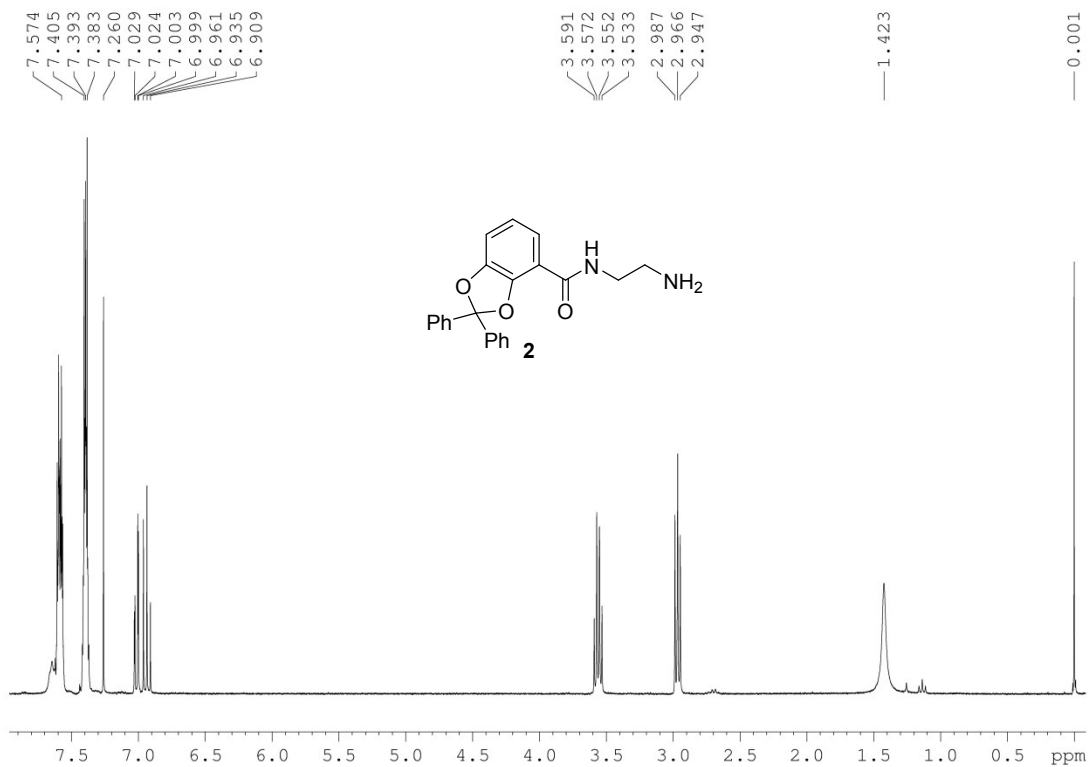
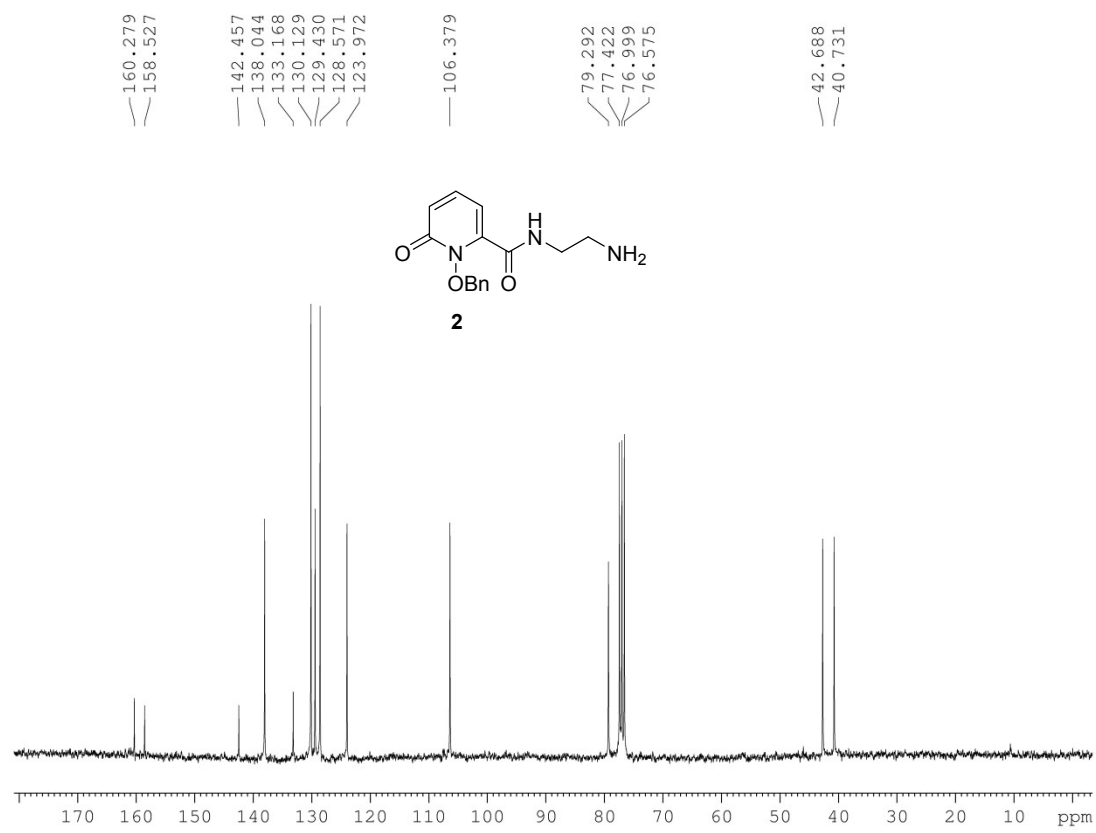
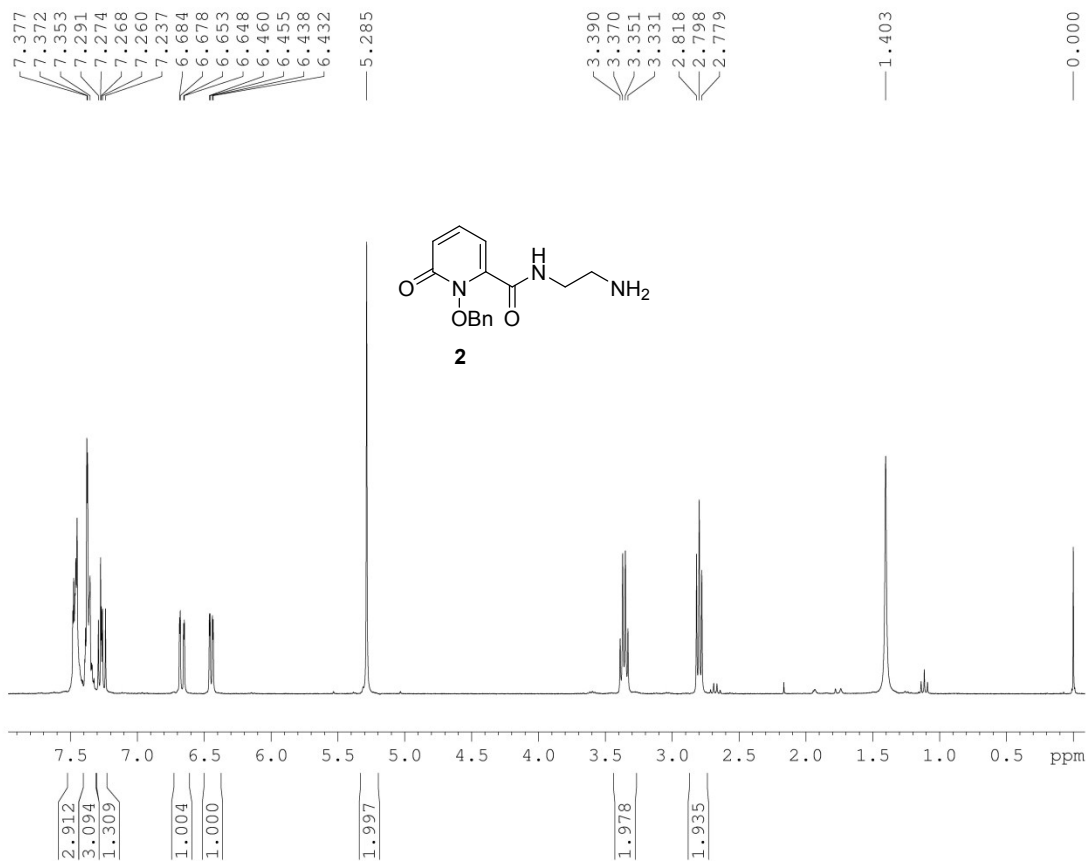


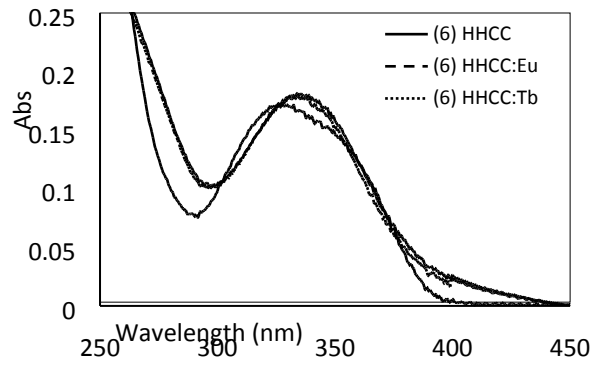
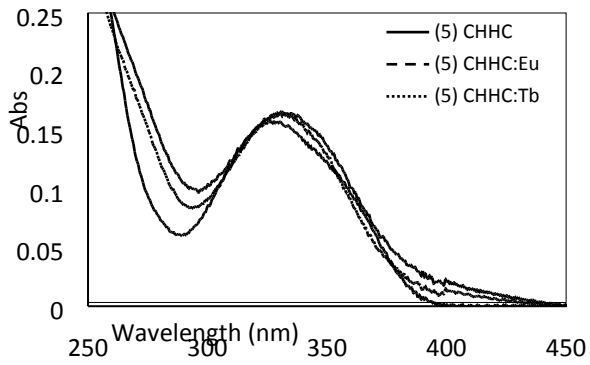
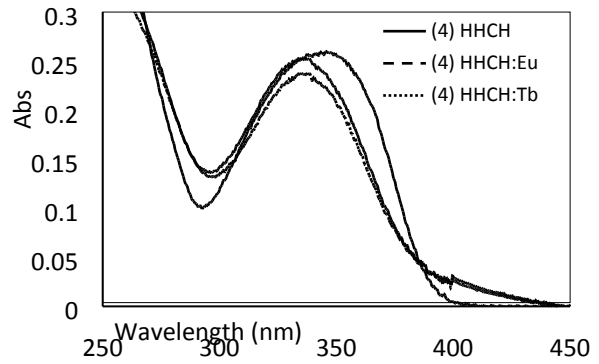
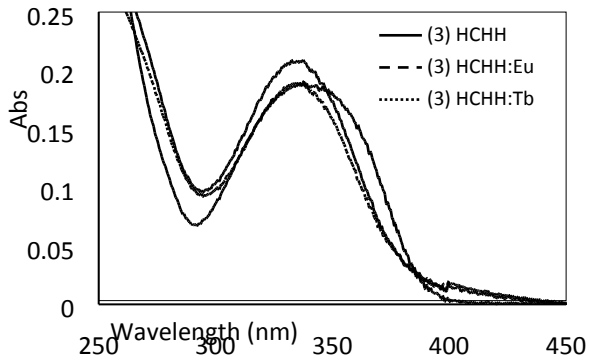
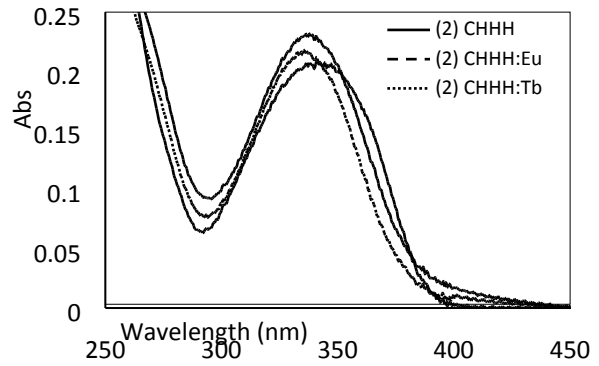
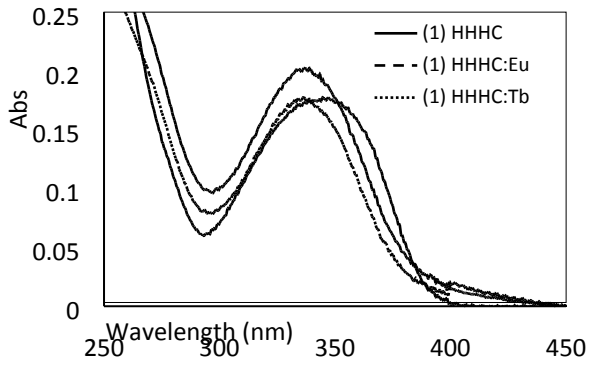
Figure S23. TOF MS-MS analysis of peptoids (8), (9), and (15). Positive mode TOF MS/MS of CCCC (15) (**top**), HCCH (9) (**middle**), and HCHC (8) (**bottom**). Fragmentation of molecular ions and masses of interest are shown. Differences in peptoids are illustrated based on both composition and sequence. H and C units differ by a mass of 1 amu.

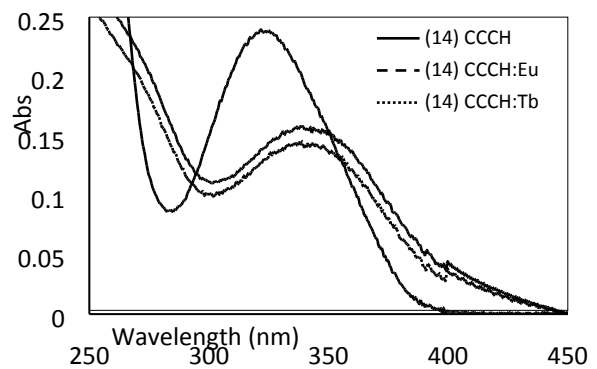
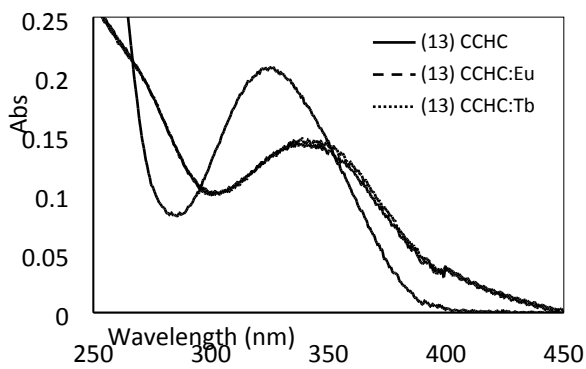
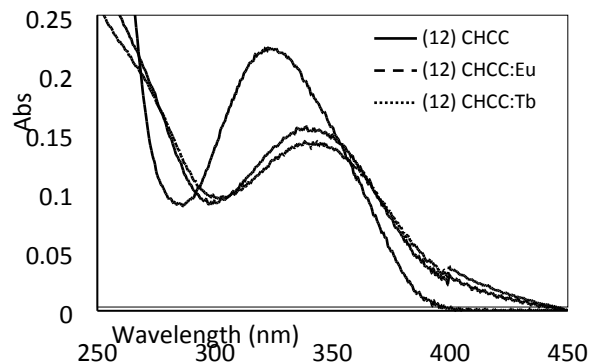
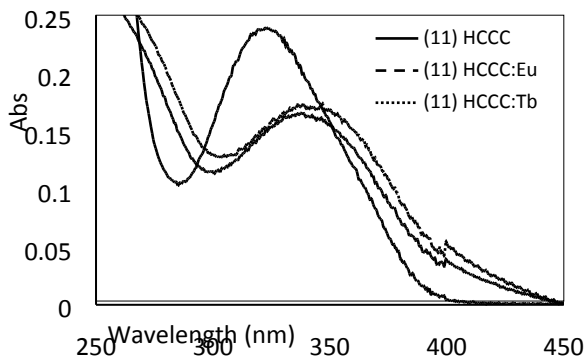
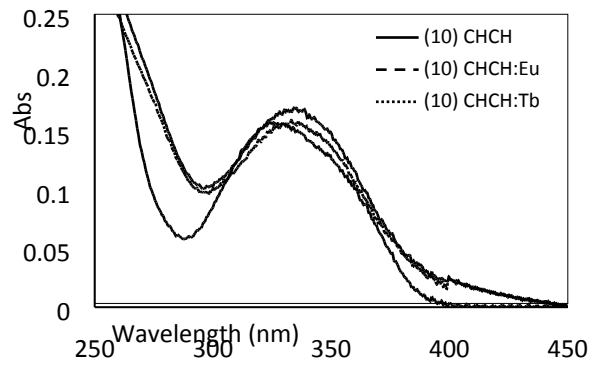
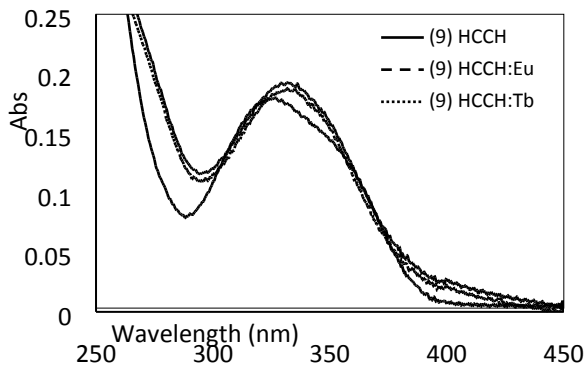
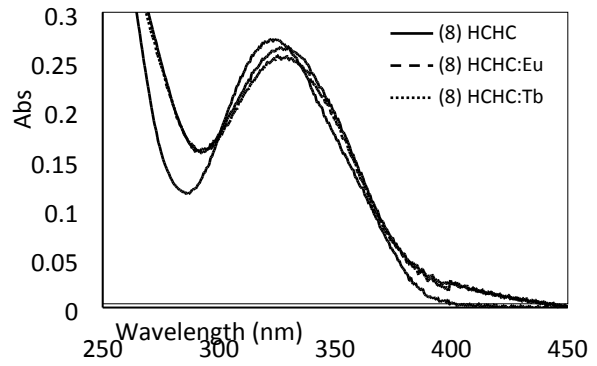
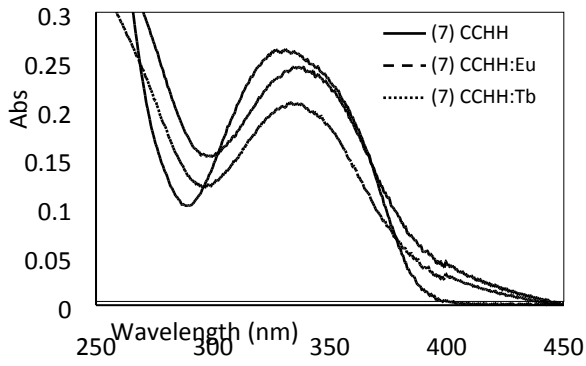
III. NMR Data





IV. UV-Vis Data





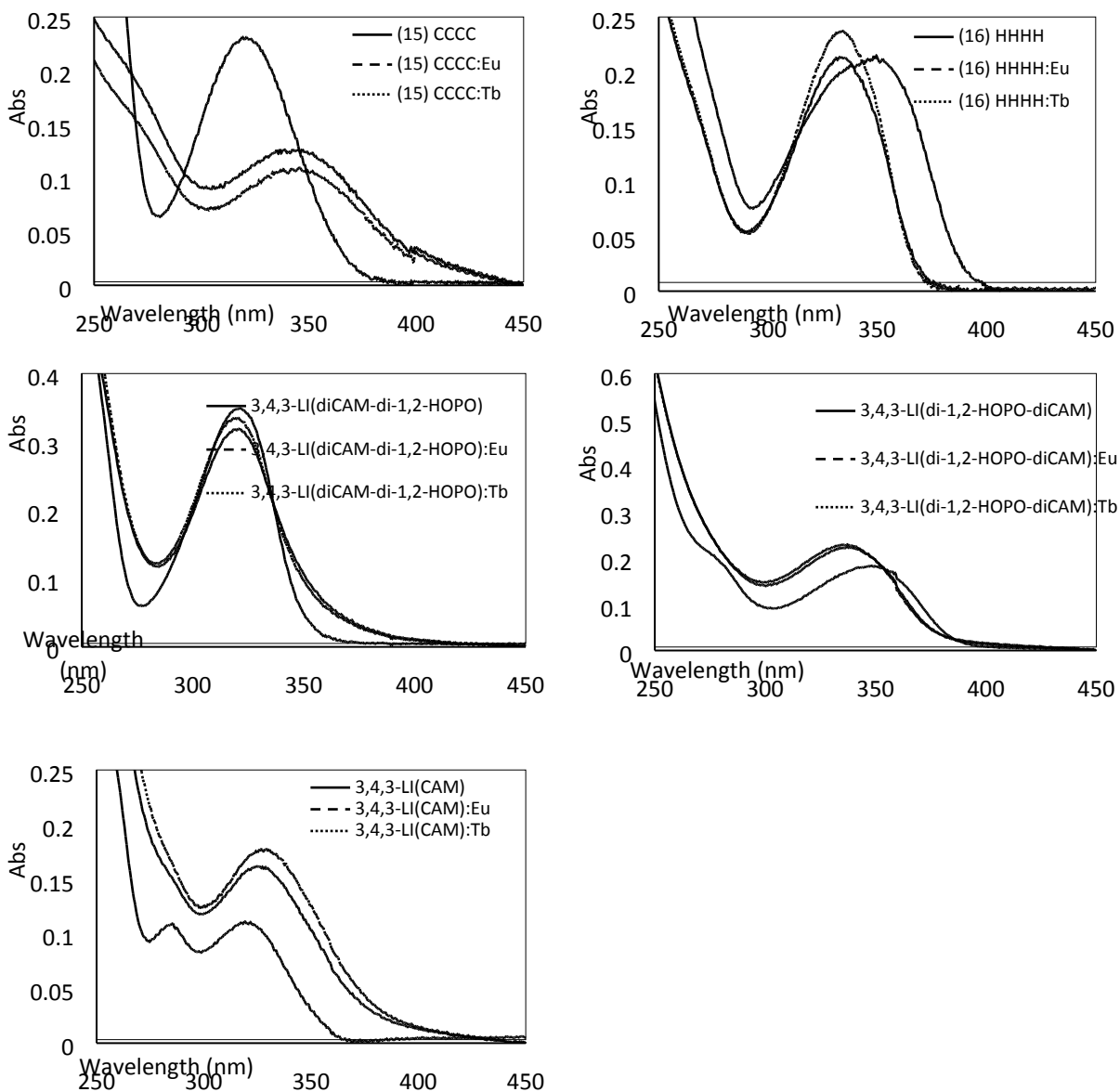
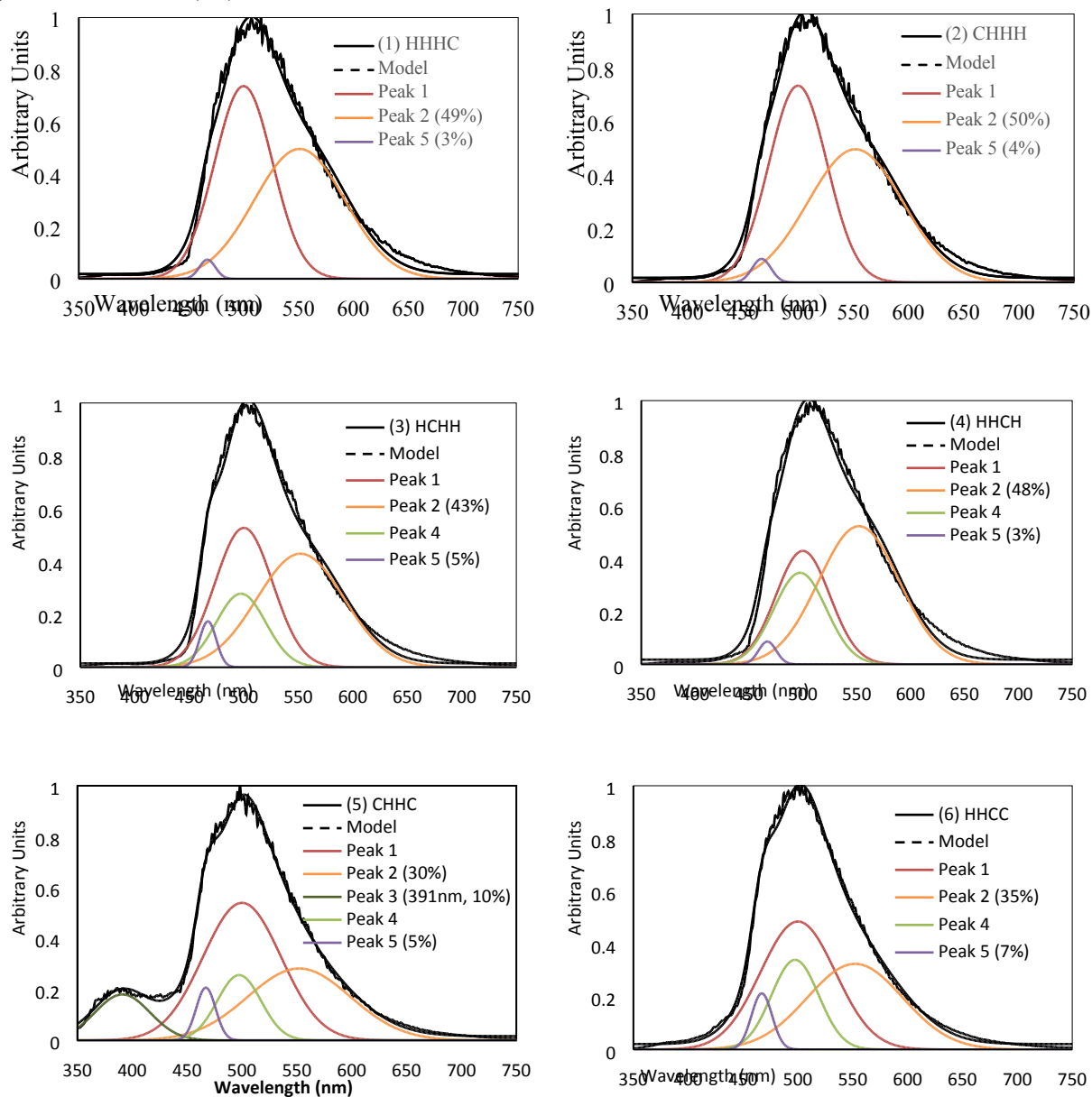


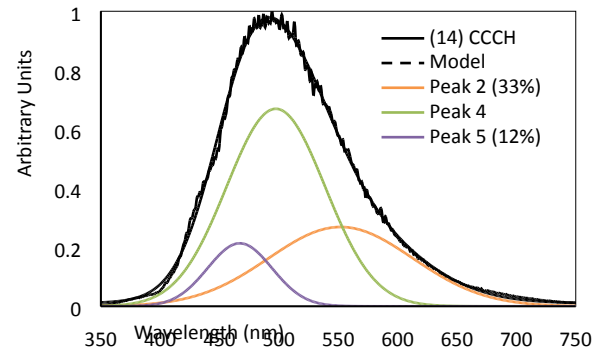
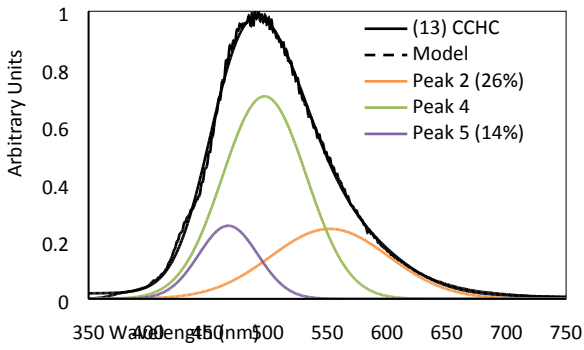
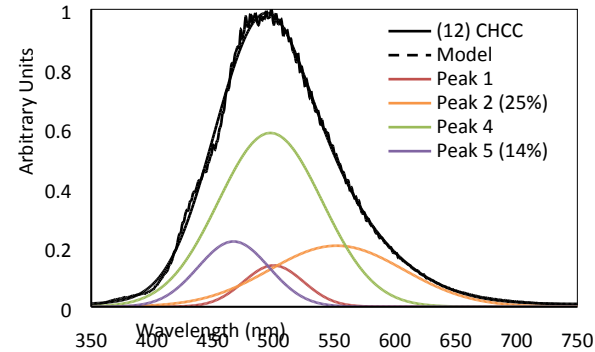
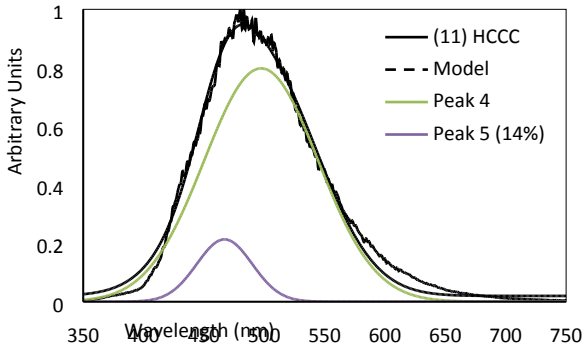
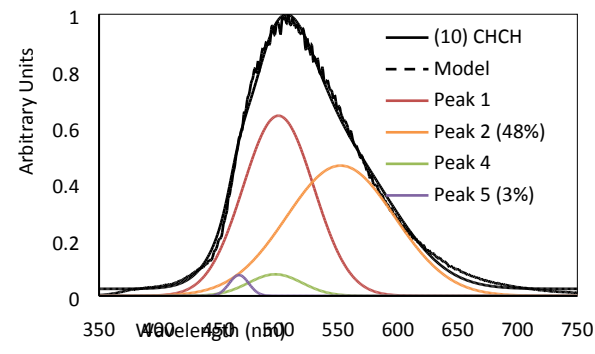
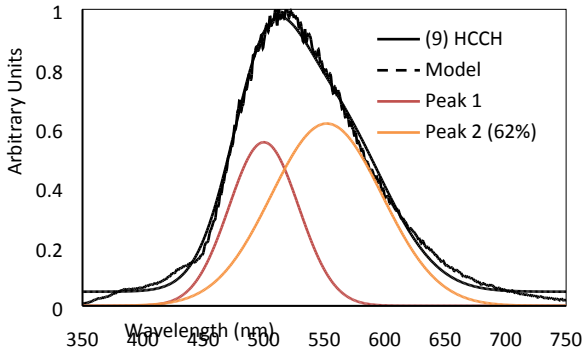
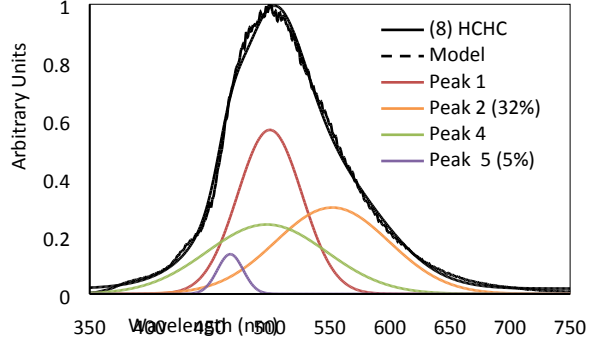
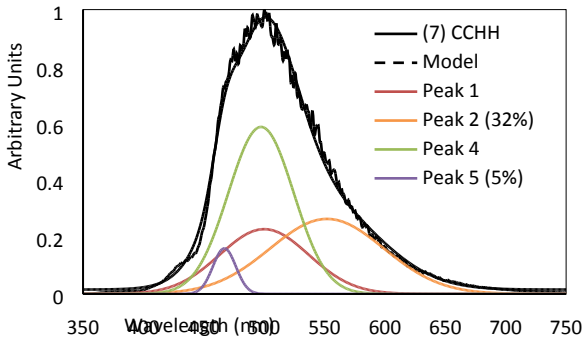
Figure S24. UV-Vis spectra for all ligands and respective Eu(III) and Tb(III) complexes.

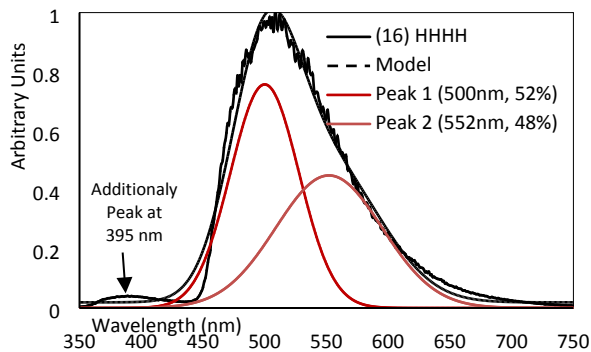
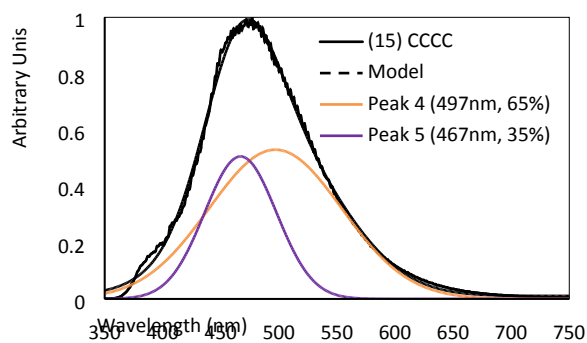
V. Luminescence Data

Triplet-State Deconvolution

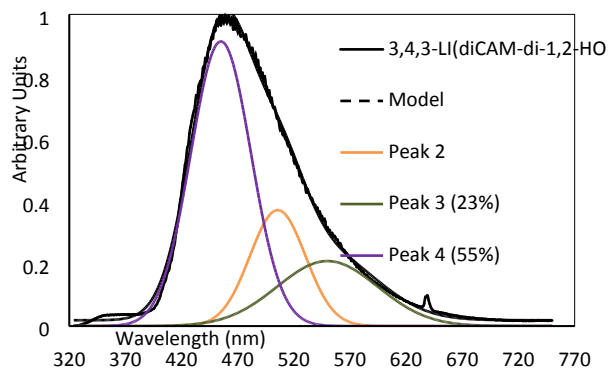
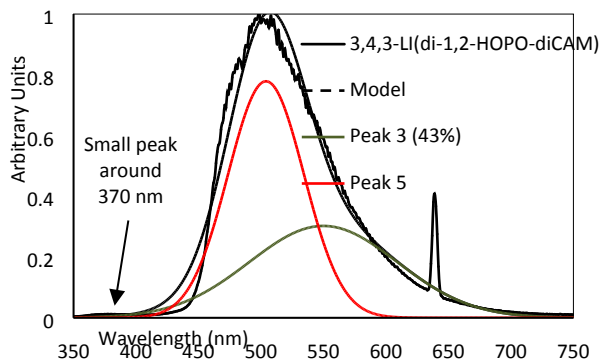
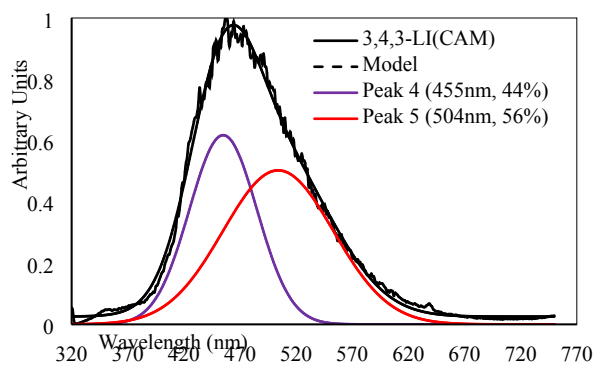
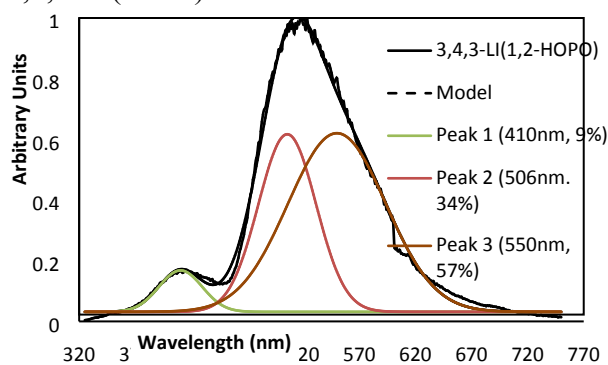
The triplet-state of (15) CCCC and (16) HHHH was deconvoluted by fitting the phosphorescence spectra of the respective gadolinium complexes with Gaussian curves. The resulting Gaussian curves were then used to model peptoids (1)-(14). Peaks 1 – 3 correspond to (16) HHHH and peaks 4 and 5 to (15) CCCC.







Similar to the peptoids, the triplet-state of 3,4,3-LI(1,2-HOPO) and 3,4,3-LI(CAM) were deconvoluted and used to model the triplet-state of 3,4,3-LI(CAM)₂(1,2-HOPO)₂ and 3,4,3-LI(1,2-HOPO)₂(CAM)₂ (referred to as 3,4,3-LI(CHHC) and 3,4,3-LI(HCCH), respectively, hereafter). Peaks 1 – 3 correspond to 3,4,3-LI(1,2-HOPO) whereas peaks 4 and 5 correspond to 3,4,3-LI(CAM).



Eu(III) Luminescence Spectra

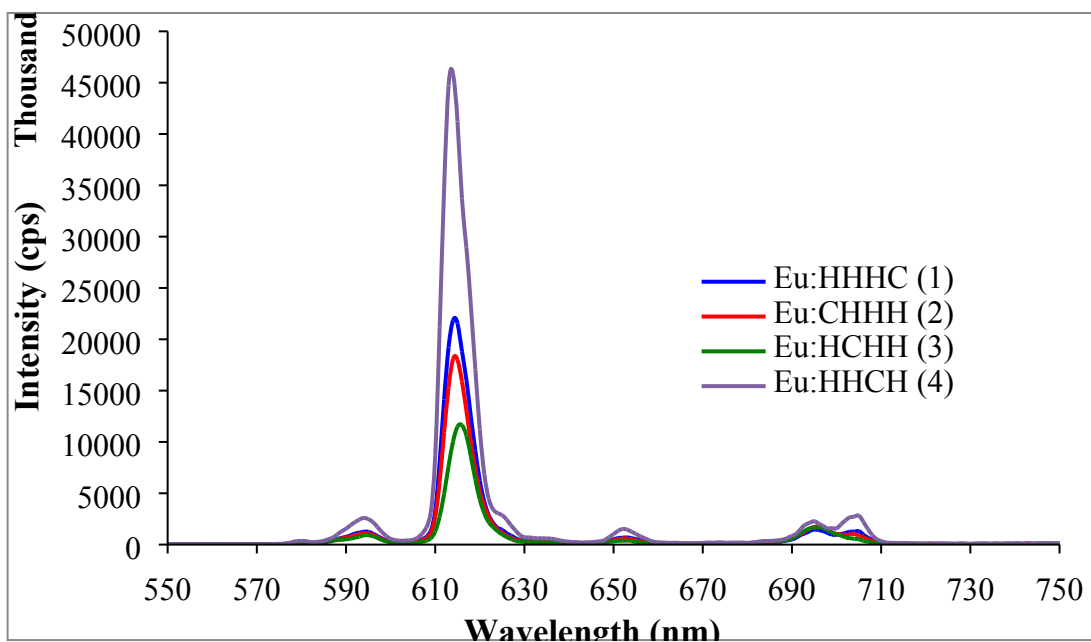


Figure S25. Eu(III) emission spectra for peptoids (1)-(4) upon excitation at 340 nm.

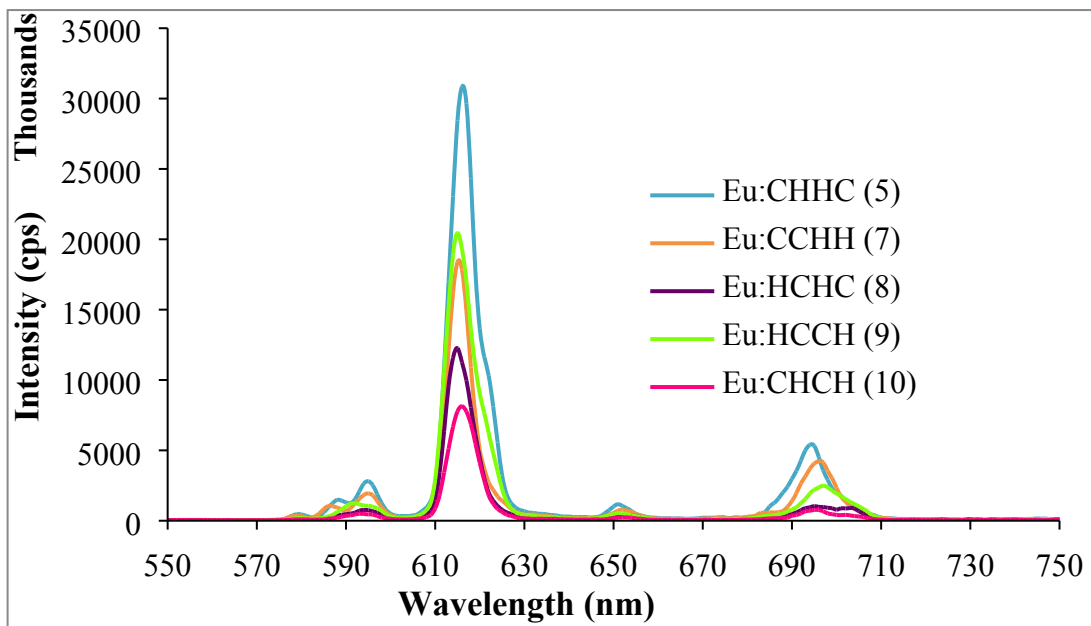


Figure S26. Eu(III) emission spectra for peptoids (5)-(10) upon excitation at either 340 nm (Eu(III)-HCHC (8); Eu(III)-CHCH (10)), 342 nm (Eu-CHHC (5)), or 345 nm (Eu(III)-CCHH (7); Eu(III)-HCCH (9)). (6) was not prepared in large enough quantities to enable full luminescence emission analysis.

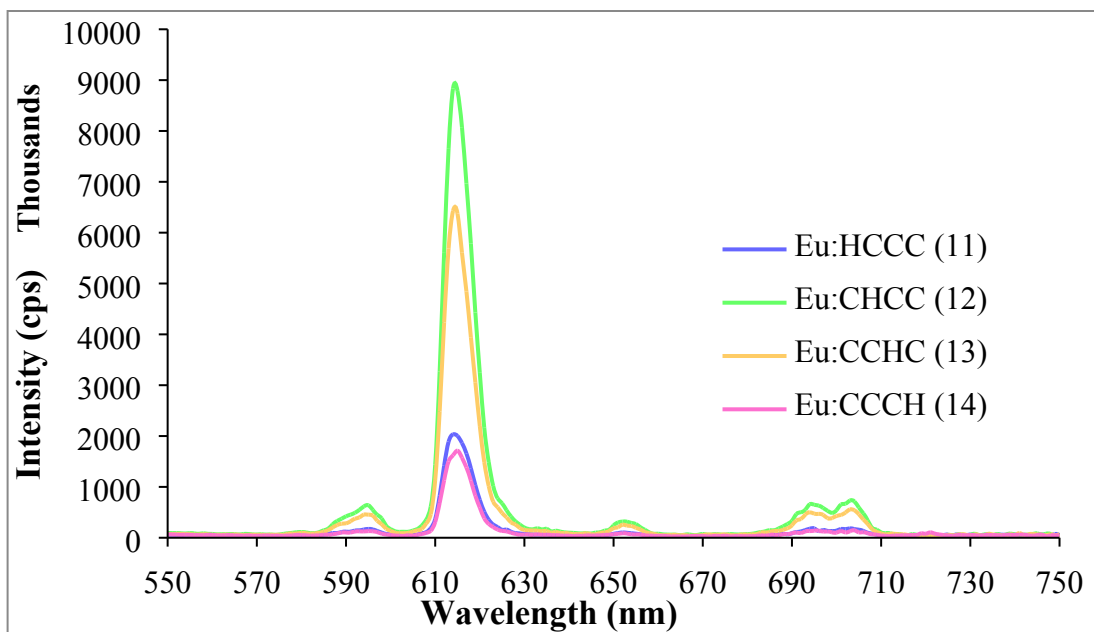


Figure S27. Eu(III) emission spectra for peptoids (11)-(14). Data is not included for (15) as CCCC did not sensitize Eu luminescence.

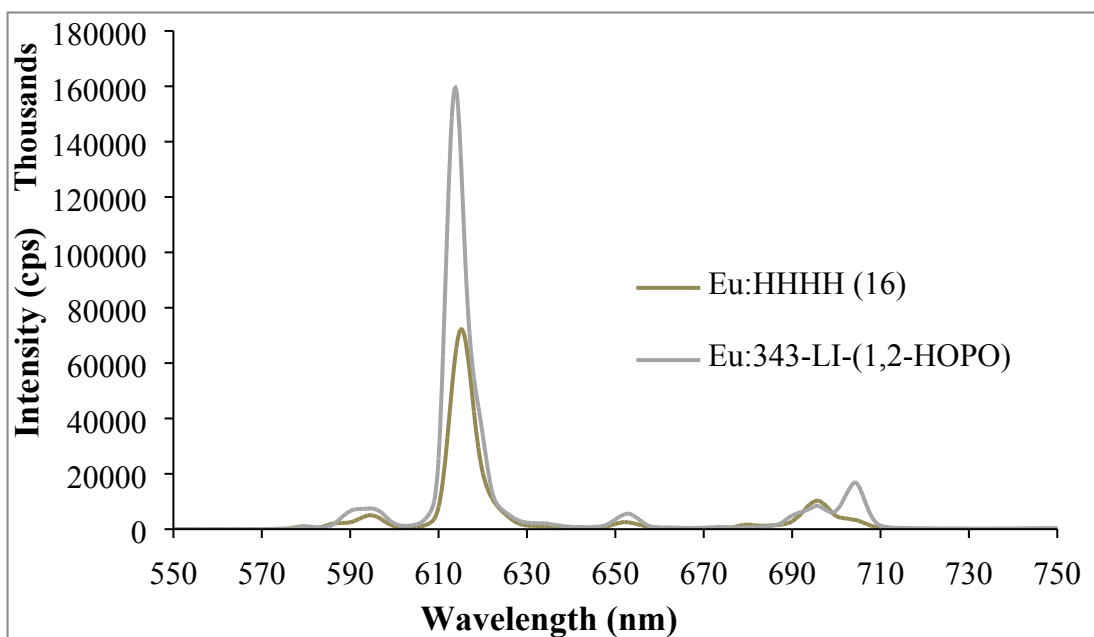


Figure S28. Eu(III) emission spectra for peptoid (16) and 3,4,3-LI-(1,2-HOPO) upon excitation at either 315 nm (Eu(III)-3,4,3-LI-(1,2-HOPO)) or 340 nm (Eu(III)-HHHH (16)).

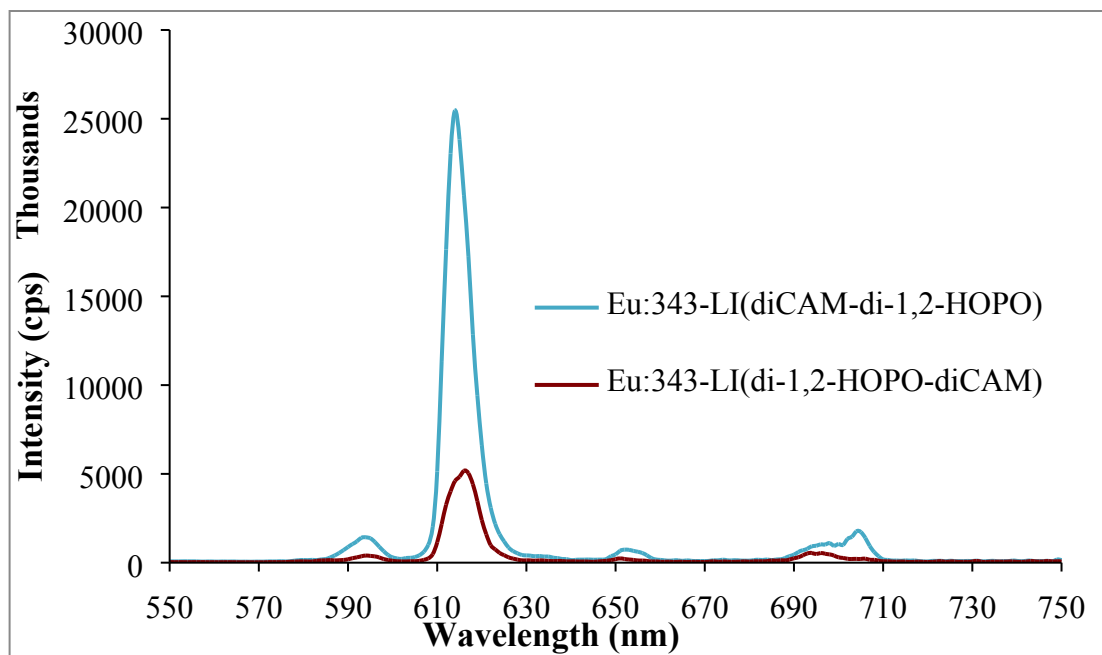
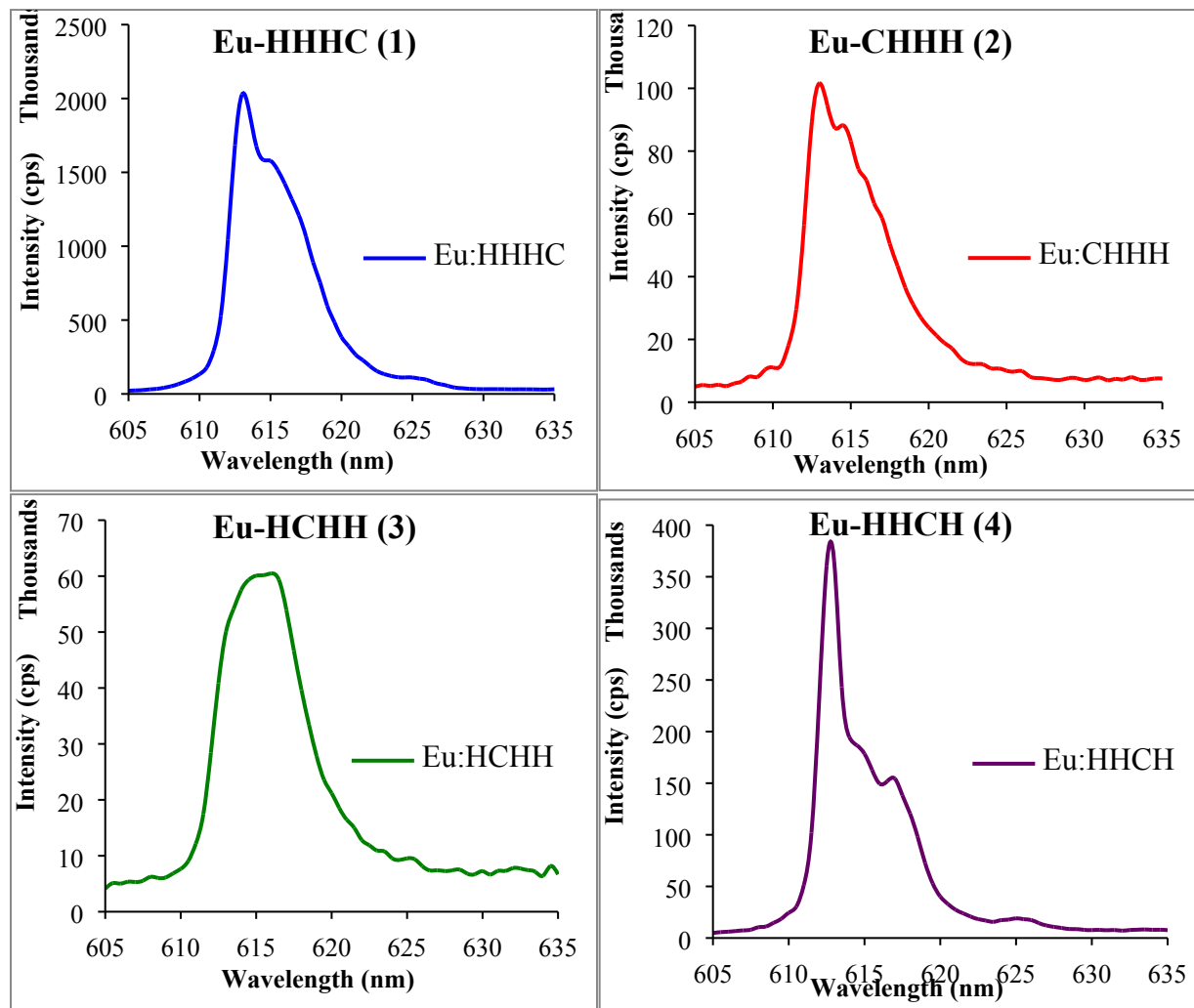
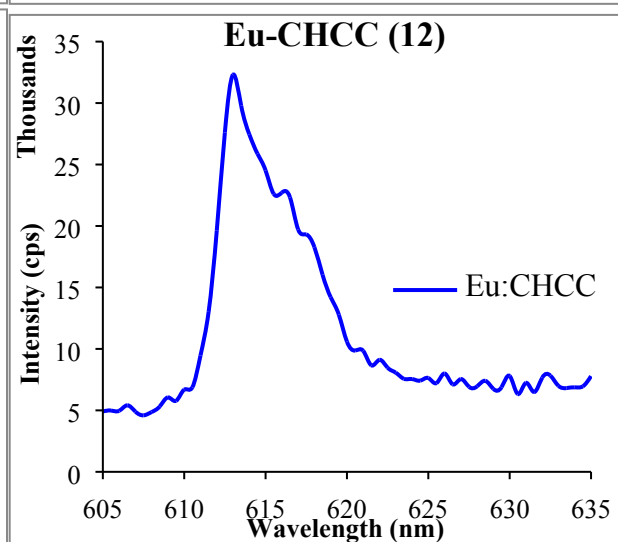
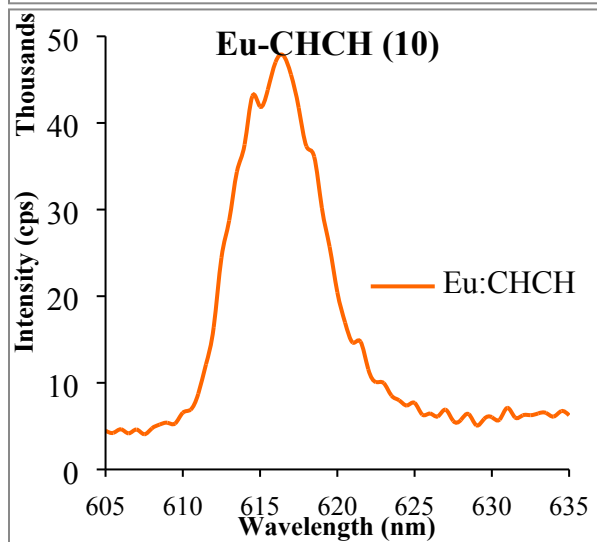
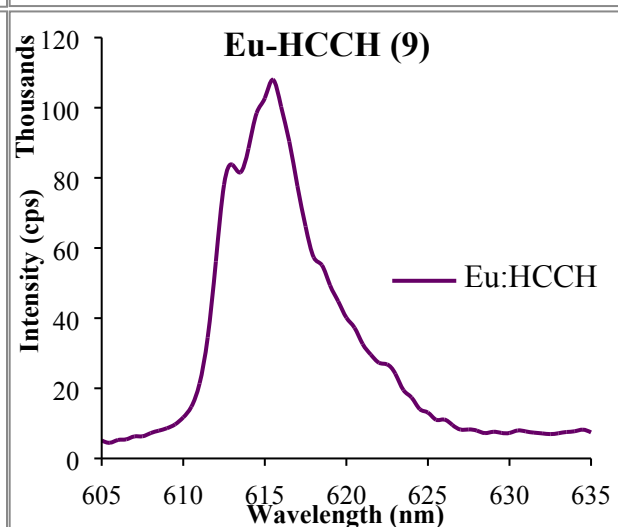
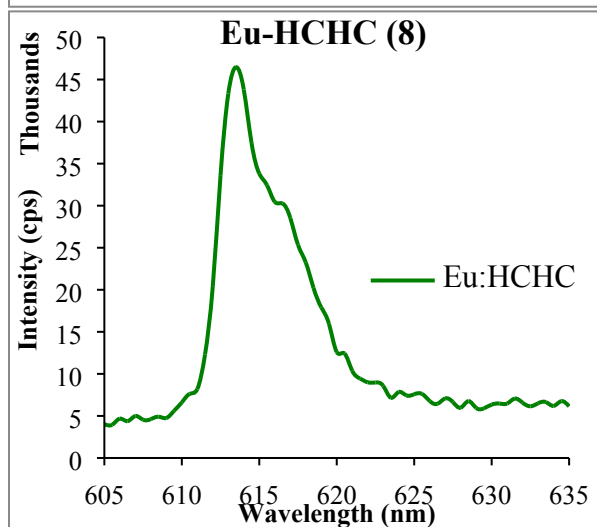
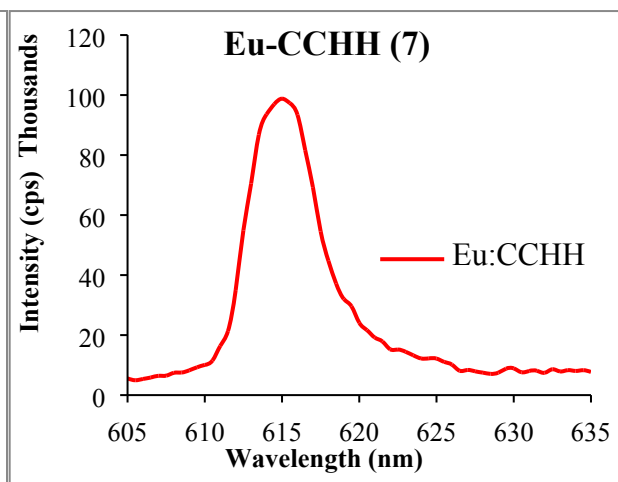
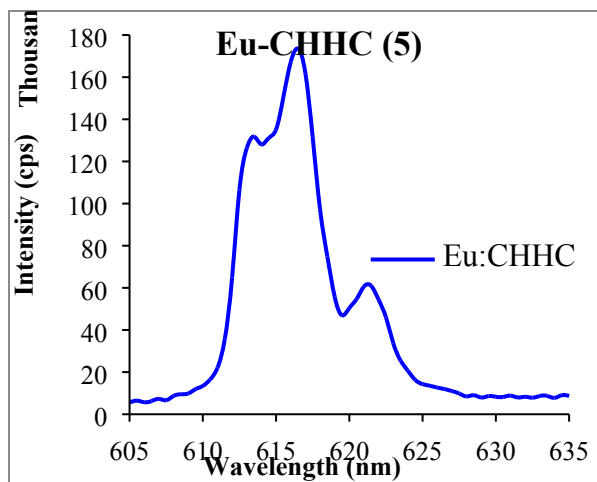
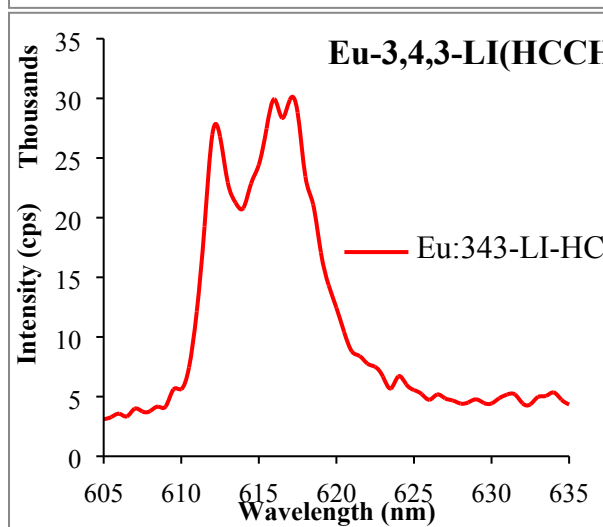
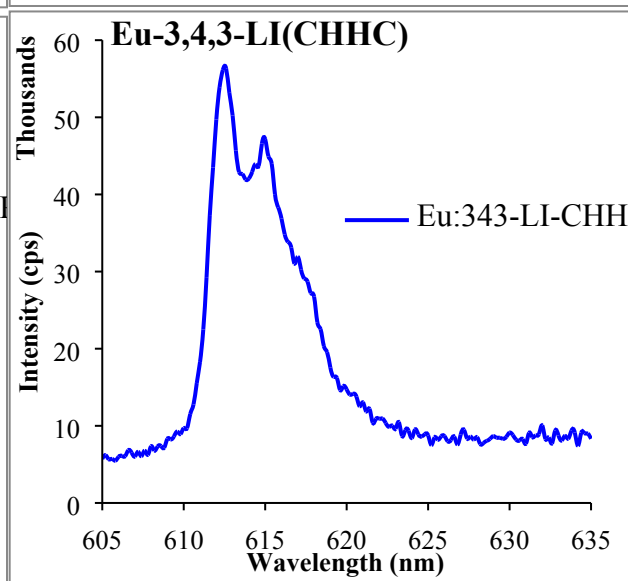
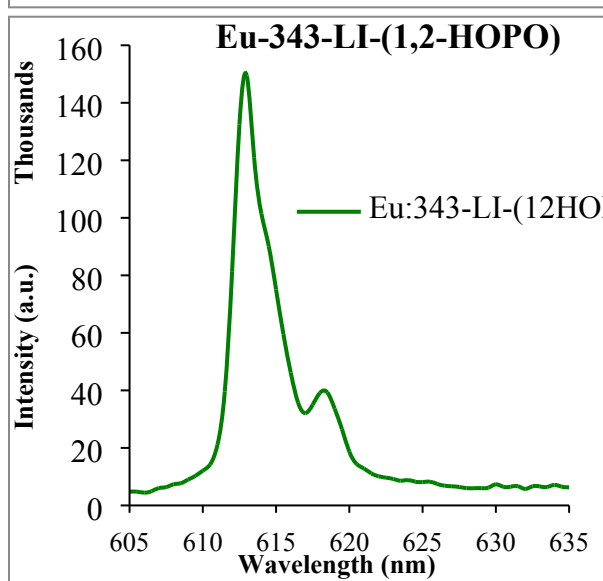
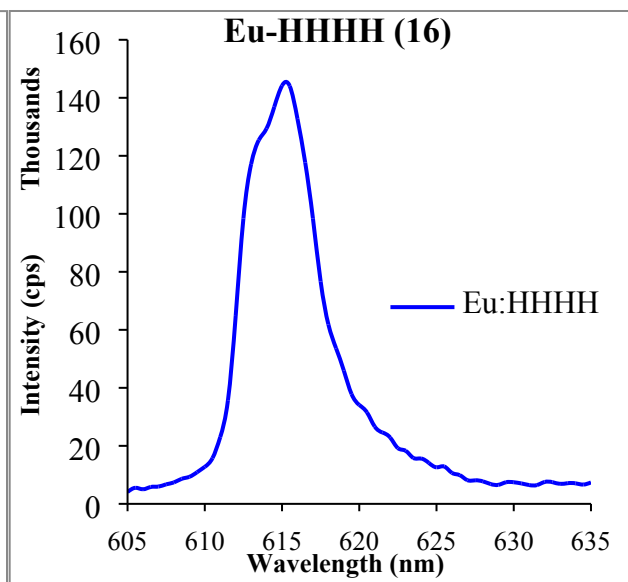
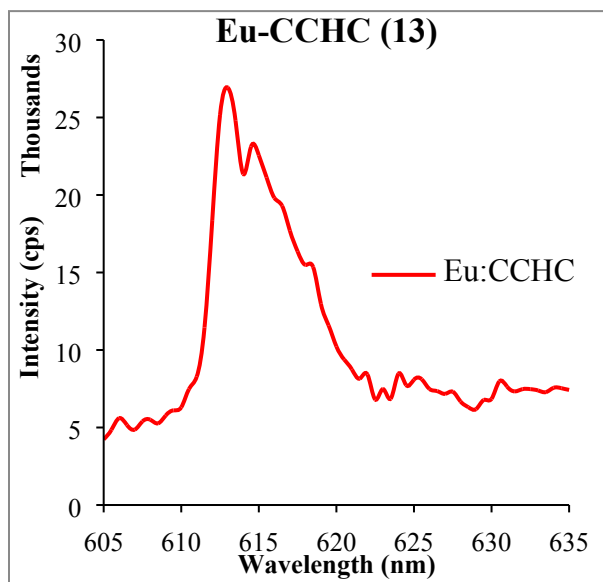


Figure S29. Eu(III) emission spectra for 3,4,3-LI(CHHC) [blue] and 3,4,3-LI(HCCH) [red] upon excitation at either 318 nm (Eu(III)-3,4,3-LI(CHHC) or 340 nm (Eu(III)- 3,4,3-LI(HCCH)).

Figure S30. High-resolution Eu(III) emission spectra for $^5D_0 \rightarrow ^7F_2$ hypersensitive transition. All the following spectra were acquired at 0.5 nm increments with 1 nm emission and excitation slits and a three second integration time. Spectral data for complexes of peptoids (11) and (14) did not show anything above background in high resolution mode. Data were not acquired for peptoids (6) and (15) as (6) was not available and (15) did not sensitize Eu luminescence.







Quantum Yield

Quantum yields were determined by the optical dilution method² using quinine sulfate as a reference and equation S1. The subscripts **r** and **s** refer to the reference quinine sulfate and the investigated sample, respectively. The variable **A** is absorbance at wavelength λ , **I** is intensity of the excitation light λ , **n** is index of refraction, and **D** is the integrated emission intensity. Both indexes of refraction were assumed to be equivalent as both samples were aqueous. Likewise, the intensities of the excitation wavelength were taken to be identical since the same excitation wavelengths (318 nm for Tb:3,4,3-LI(CHHC) and 347 nm for Eu:HHCH (4)) were used for a given **r** and **s**. Therefore, plotting the integrated intensity against absorbance yields a slope that can be equated to the quantum yield, ϕ . By using the reported quantum yield of quinine sulfate ($\phi_r = 0.546$) and taking the ratio of the slopes and quantum yield for **s** and **r**, the quantum yield of the sample was determined. A representative plot for Tb:3,4,3-LI(CHHC) and Eu:HHCH (4) is reported in Figure S30. Only the slope was used since the y-intercept was at least two-orders of magnitude lower than the slope.

$$\frac{\Phi_s}{\Phi_r} = \frac{A_r(\lambda_r)I(\lambda_r)n_s^2D_s}{A_s(\lambda_s)I(\lambda_s)n_r^2D_r} \quad (\text{S1})$$

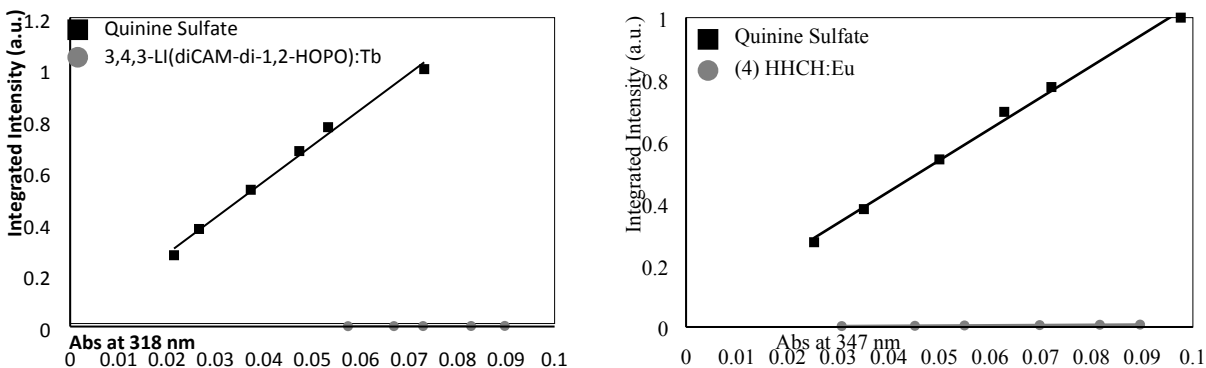


Figure S31. Representative dilution curves used to determine quantum yield values. On the left and right are plots for Tb:3,4,3-LI(CHHC) and Eu:HHCH (4), respectively. The black squares represent the reference quinine sulfate and the gray circles the investigated sample.

Table S1. Estimated quantum yield values unless otherwise noted. * Indicates the value was acquired via the optical dilution method using three independent trials.

Ligand	□	
	Eu ³⁺	Tb ³⁺
(1) HHHH	0.021	ND
(2) CHHH	0.018	ND
(3) HCHH	0.012	ND
(4) HHCH	0.043±0.002*	ND
(5) CHHC	0.035	ND
(6) HHCC	ND	ND
(7) CCHH	0.021	ND
(8) HCHC	0.012	ND
(9) HCCH	0.023	ND
(10) CHCH	0.0083	ND
(11) HCCC	0.0020	ND
(12) CHCC	0.0093	ND
(13) CCHC	0.00015	ND
(14) CCCH	0.0016	ND
(15) CCCC	NA	ND
(16) HHHH	0.074	ND
3,4,3-LI(1,2-HOPO)	0.14	ND
3,4,3-LI(CAM)	NA	ND
3,4,3-LI(HCCH)	0.0057	NA
3,4,3-LI(CHHC)	0.023	0.0011±0.0001*

Luminescence Lifetimes

Lifetime data for Ln(III)-peptoid and 3,4,3-ligand complexes was acquired by exciting complexes at their respective excitation maxima and monitoring the hypersensitive transition (i.e. $^5D_0 \rightarrow ^7F_2$ for Eu^{3+} and $^5D_4 \rightarrow ^7F_5$ for Tb^{3+}). Data were analyzed and fitted using the DAS 6 decay analysis software package by minimizing chi-squared values and monitoring the shape and amplitude of data residuals. Each of the complexes was modeled with biexponential decays except for Eu:HHCH (4) and Eu:CHHC (5) where one component was used and Eu:HCCC (11) and Tb:3,4,3-LI(CHHC) where three components were used. The number of water molecules found in the inner coordination sphere of the Eu(III) metal centers was determined using the hydration formula (Equation S2) published by Kimura *et al.*,³ where k_{obs} is the inverse of the measured lifetime in seconds.

$$N_{\text{H}_2\text{O}} = 1.05 * 10^{-3} * k_{\text{obs}}^{\text{Eu}} - 0.44 \quad (\text{S2})$$

Table S2. Luminescence lifetimes for Eu(III) and Tb(III)-peptoid and 3,4,3-ligand complexes. Lifetime values are reported based on one measured sample. The calculated number of water molecules (per Kimura's equation)³ were included where appropriate.

	(1) HHHC	(2) CHHH	(3) HCHH	(4) HHCH	(5) CHHC	(7) CCHH	(8) HCHC	(9) HCCH	(10) CHCH	(11) HCCC
Eu^{3+} $\tau_1/\tau_2/\tau_3$ (ms)	0.151/ 0.557	0.242/ 0.611	0.157/ 0.432	0.679	0.553	0.202/ 0.448	0.131/ 0.543	0.257/ 0.474	0.161/ 0.425	0.073/ 0.127/ 0.569
$N_{1,\text{H}_2\text{O}}/N_{2,\text{H}_2\text{O}}$	6.5/1.4	3.9/1.3	6.2/2.0	1.1	1.5	4.8/1.9	7.6/1.5	3.6/1.8	6.1/2.0	--/7.8/ 1.4
	(13) CCHC	(14) CCCH	(15) CCCC	(16) HHHH						
Eu^{3+} $\tau_1/\tau_2/\tau_3$ (ms)	0.331/ 0.682	0.308/ 0.665	0.014/ 0.778	0.119/ 0.827						
$N_{1,\text{H}_2\text{O}}/N_{2,\text{H}_2\text{O}}$	2.7/1.1	3.0/1.1	--/ 0.9	8.4/0.8						

		3,4,3-LI(CAM)	3,4,3-LI(HCCH)	3,4,3-LI(CHHC)
$\tau_1/\tau_2/\tau_3$ (ms)	Eu^{3+}	—	0.121 ($N_{\text{H}_2\text{O}}=8.2$)/ 0.538 ($N_{\text{H}_2\text{O}}=1.5$)	0.267 ($N_{\text{H}_2\text{O}}= 3.5$)/ 0.733 ($N_{\text{H}_2\text{O}}= 1.0$)
	Tb^{3+}	0.070/ 0.293	—	0.050/ 0.185/ 0.456

VI. Solution Thermodynamics

All spectral data acquired for protonation and stability constants were imported to HypSpec⁴ for a nonlinear least-squares fitting. An equilibrium constant is defined as a cumulative formation constant according to equation S2, where m , l , and h are the stoichiometric coefficients of the metal (M), ligand (L), and proton (H), respectively. Spectra were corrected by a dilution factor when applicable and modeled at the initial metal and ligand concentration of the sample. The absorbance spectra for each of the protonated states of a species were assumed to be sufficiently different to allow for deconvolution via HypSpec. Each HOPO and CAM unit provides either one or two acidic hydrogen atoms, respectively, to the ligand thus protonation equilibria were modeled accordingly. The pK_a of the investigated ligands were determined and are found in Table S3. Metal hydrolysis products (from NIST database)⁵ and protonation constants were incorporated into the model to refine the values where the metal was present (i.e. $m = 1$). Cumulative formation constants (β_{mlh}) for Eu^{3+} complexes were modeled by three (β_{110} , β_{111} , β_{112}) and two (β_{110} , β_{111}) species, respectively, for data from spectrophotometric titrations. The only fluorescently active species in the batch titrations involving 3,4,3-LI(HCCH) at pH 7.4 was assumed to be $\text{Eu}:3,4,3\text{-LI}(1,2\text{-HOPO})$, based on previous characterization of the $\text{Eu}(\text{III})$ complex, and the protonated 3,4,3-LI(HCCH) europium complex (i.e. β_{111}).

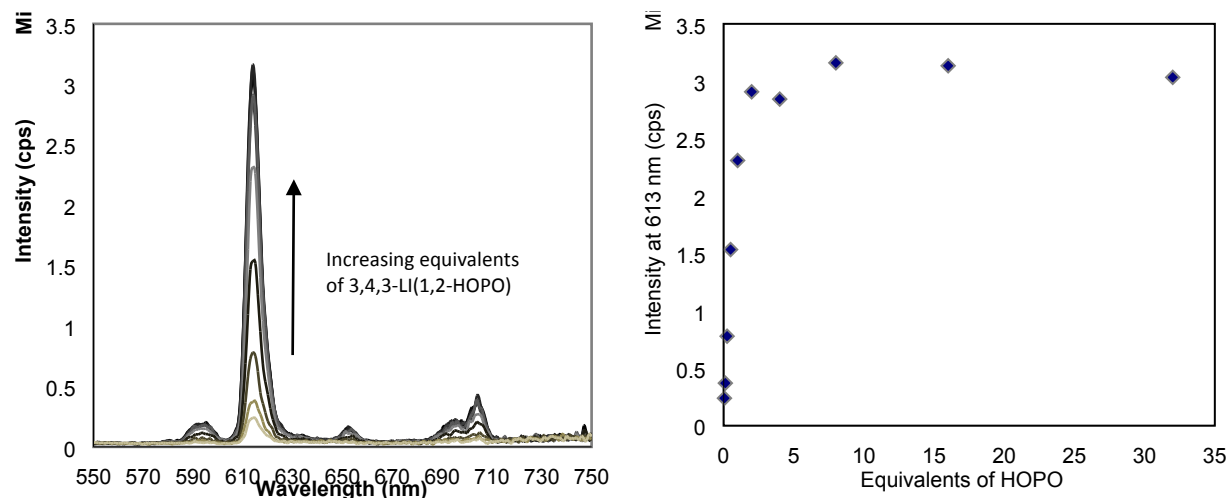
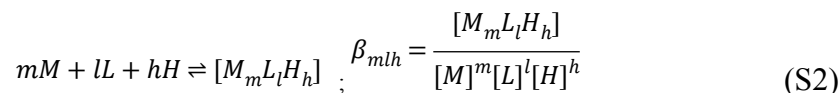


Figure S32. Representative luminescence data for competition batch titrations. Each sample had 100 nM of a precomplexed $\text{Eu}:3,4,3\text{-LI}(\text{HCCH})$ and varying equivalents of 3,4,3-LI(1,2-HOPO). All samples were buffered in 50 mM HEPES at pH 7.4, held at 0.1 M ionic strength (KCl supporting electrolyte), and incubated at 25°C. Samples were excited at 318 nm and data was refined using the HypSpec software package.

Table S3. Protonation and stability constants for selected ligands and complexes. The errors correspond to the standard deviation from three independent titrations unless otherwise noted. All data was collected at 25°C from aqueous solutions held at 0.1 M ionic strength (KCl supporting electrolyte). ^aValue were held constant during data refinement. ^bValue were based on two independent trials. ^cValue obtained via fluorimetric batch titrations.

Species	<i>mlh</i>	$\log(\beta_{mlh})$ (7) CCHH	pK_a	Species	<i>mlh</i>	$\log \beta_{mlh}$ (15) CCCC	pK_a
LH ⁵⁻	011	12.5 ^a	12.5 ^a	LH ⁷⁻	011	13 ^a	13 ^a
LH ₂ ⁴⁻	012	23.52 ± 1.42	10.75 ± 1.42	LH ₂ ⁶⁻	012	25 ^a	12 ^a
LH ₃ ³⁻	013	32.21 ± 2.32	8.95 ± 1.01	LH ₃ ⁵⁻	013	36 ^a	11 ^a
LH ₄ ²⁻	014	39.59 ± 2.93	7.39 ± 0.68	LH ₄ ⁴⁻	014	45.51 ± 0.45	9.51 ± 0.45
LH ₅ ⁻	015	44.82 ± 3.23	5.22 ± 0.44	LH ₅ ³⁻	015	53.80 ± 0.88	8.28 ± 0.44
LH ₆	016	48.61 ± 3.30	3.79 ± 0.31	LH ₆ ²⁻	016	60.84 ± 1.34	7.04 ± 0.47
				LH ₇ ⁻	017	66.07 ± 1.84	5.23 ± 0.50
				LH ₈	018	68.47 ± 2.36	2.40 ± 0.53
[EuL] ³⁻	110	36.01 ± 4.13		[EuL] ⁵⁻	110	28.88 ± 3.45	
[EuLH] ²⁻	111	43.05 ± 3.22		[EuLH] ⁴⁻	111	39.26 ± 2.97	
[EuLH ₂] ⁻	112	47.08 ± 2.47		[EuLH ₂] ³⁻	112	45.48 ± 2.80	
		3,4,3-LI(CHHC)				3,4,3-LI(HCCH)	
LH ⁵⁻	011	15.02 ± 0.70 ^b	>12 ^{a, b}	LH ⁵⁻	011	12.5 ^a	12.5 ^a
LH ₂ ⁴⁻	012	26.56 ± 0.16 ^b	11.54 ± 0.55 ^b	LH ₂ ⁴⁻	012	24.5 ^a	12 ^a
LH ₃ ³⁻	013	35.60 ± 0.01 ^b	9.03 ± 0.17 ^b	LH ₃ ³⁻	013	36.26 ± 0.17	11.76 ± 0.17
LH ₄ ²⁻	014	43.18 ± 0.03 ^b	7.59 ± 0.04 ^b	LH ₄ ²⁻	014	44.96 ± 0.20	8.70 ± 0.06
LH ₅ ⁻	015	48.90 ± 0.07 ^b	5.72 ± 0.07 ^b	LH ₅ ⁻	015	49.99 ± 0.20	5.03 ± 0.05
LH ₆	016	53.35 ± 0.19 ^b	4.44 ± 0.12 ^b	LH ₆	016	53.73 ± 0.28	3.74 ± 0.10
[EuL] ³⁻	110	35.97 ± 0.06					
[EuLH] ²⁻	111	45.69 ± 0.29		[EuLH] ²⁻	111	43.34 ± 0.49 ^c	
[EuLH ₂] ⁻	112	51.50 ± 0.14					

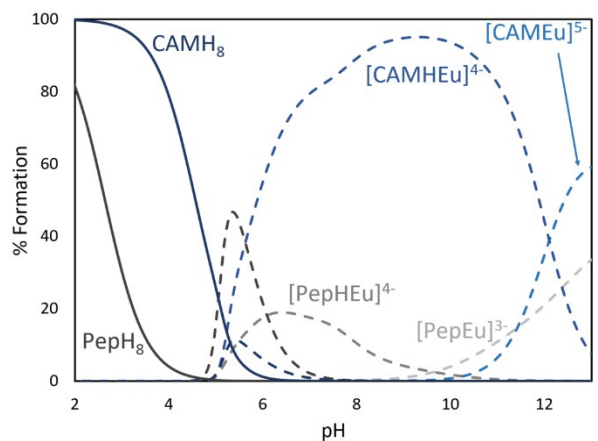


Figure S33. Eu^{3+} binding competition between (15) CCCC and 3,4,3-LI(CAM) abbreviated Pep (gray) and CAM (blue), respectively. $[\text{Pep}] = [\text{CAM}] = [\text{Metal}] = 25 \mu\text{M}$, $I = 0.1 \text{ M}$, $T = 25 \text{ }^\circ\text{C}$. Only the major species were labeled on the plots for clarity. Solid lines correspond to free ligand and dashed lines indicate complexed species. Data calculated using HySS software.⁶

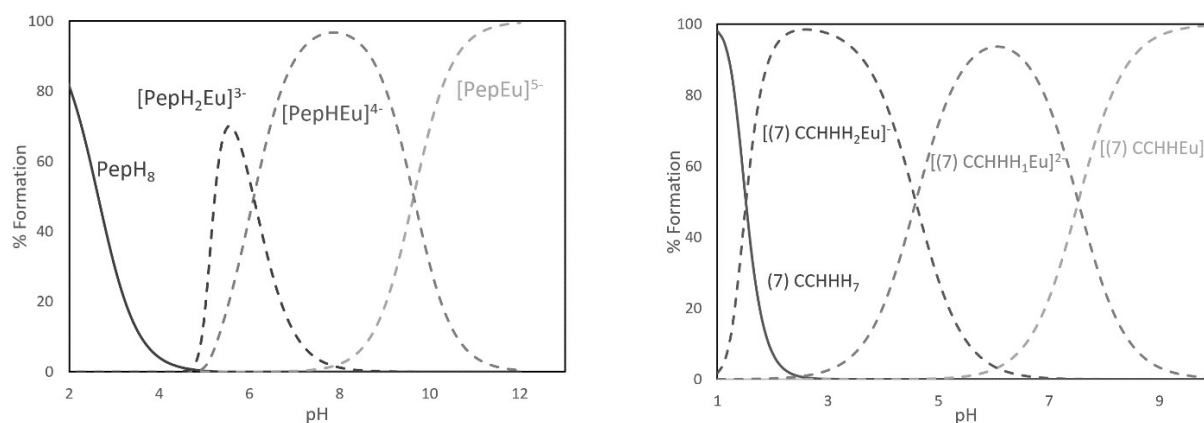


Figure S34. Eu^{3+} binding and speciation with (15) CCCC (left) and (7) CCHH (right). CCCC is abbreviated as “Pep” on the graph. $[(15) \text{ CCCC}] = [(7) \text{ CCHH}] = [\text{Eu}^{3+}] = 25 \mu\text{M}$, $I = 0.1 \text{ M}$, $T = 25 \text{ }^\circ\text{C}$. Solid lines correspond to free ligand and dashed lines indicate complexed species. Data calculated using HySS software.⁶

VII. References

- (1) E. Baco, F. Hoegy, I. J. Schalk and G. L. A. Mislin, *Org. Biomol. Chem.*, 2014, **12**, 749–757.
- (2) R. J. Abergel, A. D’Aléo, C. Ng Pak Leung, D. K. Shuh and K. N. Raymond, *Inorg. Chem.*, 2009, **48**, 10868-10870.
- (3) T. Kimura, R. Nagaishi, Y. Kato and Z. Yoshida, *J. Alloys. Compd.*, 2001, **323-324**, 164-168.
- (4) P. Gans, A. Sabatini, and A. Vacca, *Talanta* 1996, **43**, 1739–1753.
- (5) A. E. Martell, R. M. Smith, and R. J. Motekaitis, *NIST46 Standard Reference Database*; National Institute of Standards and Technology: Gaithersburg, MD, 2004.
- (6) L. Alderighi, P. Gans, A. Ienco, D. Peters, A. Sabatini, and A. Vacca, *Coord. Chem. Rev.*, 1999, **184**, 311–318.